Morphometric Characterization of Limbal Vasculature using Ultra-high Resolution Optical Coherence Tomography

by

Emmanuel Borquaye Alabi

A thesis

presented to the University of Waterloo

in fulfillment of the

thesis requirement for the degree of

Master of Science

in

Vision Science

Waterloo, Ontario, Canada, 2013

AUTHOR'S DECLARATION

I hereby declare that I am the sole author of this thesis. This is a true copy of the thesis, including any required final revisions, as accepted by my examiners.

I understand that my thesis may be made electronically available to the public.

Abstract

Purpose: The aim of the present study was to compare and investigate morphometric characteristics of limbal vasculature within the superior and inferior limbal regions using ultra-high resolution optical coherence tomography.

Method: Cross-sectional images of the human corneo-scleral limbus were acquired with a research grade ultra-high resolution optical coherence tomographer (UHR-OCT) from 14 healthy subjects after manual retraction of the upper and lower eyelid. The UHR-OCT provides an axial and lateral resolution in biological tissue of ~3µm and ~18µm, respectively. 3D stacks of OCT images (1000 x 1024 x 256) were acquired of the transition from cornea to bulbar conjunctiva at the superior and inferior limbal region. All visible vessels within the limbal region were measured using an Image J circle or ellipse tool. Vessel depth and size measurements were repeated for the same vessel and the concordance correlation coefficient was computed. Quantitative differences in vessel size and depth in the limbal region were analyzed using repeated measured ANOVA. R and SPSS were used for all data analysis procedures.

Results: The average vessel size for superior and inferior limbus were 29.28µm ± 17.649 µm (SD) and 23.68µm ± 18.118µm (SD) respectively. The average vessel depth for superior and inferior limbus were 176.76µm ± 108.698µm (SD) and 205.62µm ± 131.991µm (SD) respectively**.** The concordance correlation coefficient for superior and inferior limbal vessel size were 0.95 (95% CI, 0.935 to 0.964) and 0.994 (95% CI, 0.991 to 0.995) respectively, while that of vessel depth were 0.998 (95% CI, 0.997 to 0.999) and 0.998 (95% CI, 0.997 to 0.998) respectively. The vessels within the superior limbus were larger than the vessels found in the inferior limbus (RM-ANOVA POS $p = 0.004$), and the vessels within the inferior limbus were on average deeper than the vessels found within the superior limbus (RM-ANOVA POS $p = 0.042$). There was a positive linear relationship between limbal vessel depth and size within the superior and inferior limbus with a Pearson correlation coefficient of 0.803 and 0.754, respectively. There were on average 9 vessels per subject within the superior limbal region as compared to 13 vessels per subject with the inferior limbal region.

Conclusion: This study provided evidence that the UHR-OCT was capable of imaging (and therefore measuring) morphometric characteristics such as the size and depth of vessels within the limbus in a repeatable manner. A positive linear association between vessel depth and size was identified in the superior and inferior limbal regions. The results of this study suggest a definite difference in the size and depth of vessels across different positions of the limbus, and this may be indicative of adaptations to chronic hypoxia caused by the constant covering of the superior limbus by the upper eyelid.

Acknowledgements

I would like to begin by acknowledging the contribution of those individuals without whom this accomplishment would not have been possible.

I sincerely thank Drs Trefford Simpson and Natalie Hutchings for having me as a student and providing unlimited guidance and support throughout my graduate study.

I would also like to acknowledge the contributions of Drs Bizheva, Feng, and Hileeto who has been very helpful and generous. Their expertise and broad knowledge provided a framework for the successful completion of this thesis.

I must mention the interaction with students and other members of the faculty enabled me to gain priceless experience.

Finally, I am grateful to my family, friends, and well-wishers who have provided the necessary support to see me through.

Table of Contents

AUTHOR'S DECLARATION ii
Abstract iii
Acknowledgements iv
Table of Contents v
List of Figures vii
List of Tables viii
Chapter 1 1.0 Introduction 1
1.1 Background 1
1.2 Purpose of the study 2
1.3 Research questions 3
Chapter 2 2.0 Literature overview 4
2.1.1 Anatomy of the limbus 4
2.1.2 Macro structure 5
2.2 Epithelium across the limbus 7
2.2.1 Corneal epithelium 7
2.2.2 Limbal epithelium 7
2.3 Limbal vasculature 8
2.3.1 Conjunctival supply 8
2.3.2 Episcleral and scleral supply 10
2.3.3 Venous outflow 10
2.4 Blood flow and regulation in the limbus 10
2.4.1 Nerves of the limbus 12
2.5 Visualization of the limbal region 12
2.5.1 SLB and gonioscopy 13
2.5.2 Confocal microscopy 13
2.5.3 Ultrasound biomicroscopy 14
2.6 Optical coherence tomography (OCT) 15
2.6.1 Introduction and definition of OCT 15
2.6.2 Origin of OCT 16
2.6.3 Types of OCT 17
2.6.4 Time domain OCT 17

2.6.5 Fourier domain OCT 18
2.6.6 Spectral domain OCT (SD OCT) 18
2.6.7 Swept source OCT (SS OCT) 19
Chapter 3 Materials and methods 20
3.1 Optical Coherence Tomography 20
3.1.1 UHR-OCT calibration 21
3.2 Participants 23
3.2.1 Inclusion and exclusion criteria 23
3.3 Study procedures 23
3.3.1 Phase one - screening procedure 24
3.3.2 Phase two - pre-test procedure 24
3.3.3 Phase three - imaging procedure 24
3.3.4 Phase four - data processing and analysis 25
Chapter 4 Results 30
Chapter 5 Discussion 43
5.1 Repeatability of UHR-OCT measurements 43
5.2 Morphologic characteristics of the limbus 50
5.3 Limitations and future studies 52
Chapter 6 Conclusions 54
Appendix 63
References 64

List of Figures

Figure 1: Enface outline of the human limbus.
Figure 2: Defining the location of the limbus in an OCT tomogram.
Figure 3: The limbal vasculature.
Figure 4: Number of articles found using Scopus research database with "optical coherence tomography" as part of the publication title, abstract or keyword.
Figure 5: Schematic representation of spectral domain UHR-OCT device.
Figure 6: Spectral domain UHR-OCT device set up.
Figure 7: A summary of the data acquisition process.
Figure 8: Identifying the sclero-limbal junction in an UHR-OCT tomogram of the limbus.
Figure 9: A summary of the data processing and analysis procedures.
Figure 10: UHR-OCT tomogram of the limbal region showing vessels.
Figure 11: Repeatability of vessel size measurements in the superior limbus.
Figure 12: Repeatability of vessel size measurements in the inferior limbus.
Figure 13: Superior and inferior limbal mean vessel sizes.
Figure 14: Repeatability of vessel depth from the anterior ocular surface in the superior limbus.
Figure 15: Repeatability of vessel depth from the anterior ocular surface in the inferior limbus.
Figure 16: Superior and inferior limbal mean vessel depths.
Figure 17: Scatterplot of the relationship between vessel depth and size of the superior limbus.
Figure 18: Subject-wise correlation lines showing the relationship between vessel depth and size of the superior limbus per subject.
Figure 19: Scatterplot of the relationship between vessel depth and size of the inferior limbus.
Figure 20: Subject-wise correlation lines showing the relationship between vessel depth and size of the inferior limbus per subject.
Figure 21: Scatterplot of the relationship between vessel depth and size of the superior and inferior limbus.
Figure 22: A UHR-OCT of the human limbus.
Figure 23: Three dimensional reconstruction of a set of UHR-OCT tomograms of which the tomogram from Figure 22 forms a part of.
Figure 24: Three dimensional reconstruction of the limbus with the epithelium stripped through an oblique slice to reveal the vessel structure within the limbus.
Figure 25: A section from the three dimensional reconstruction of the limbus in Figure 24 revealing the vessel structure within the limbus from an enface view.

List of Tables

Table 1: Morphometric characteristics for the superior limbal region.

Table 2: Morphometric characteristics for the inferior limbal region.

Table 3: Legend and subject-wise correlation coefficients for the linear relationship between vessel depth and size within the superior limbus.

Table 4: Legend and subject-wise correlation coefficients for the linear relationship between vessel depth and size within the inferior limbus.

Chapter 1

1.0 Introduction

1.1 Background

The limbus is the zone that separates the opaque sclera (overlaid by transparent conjunctiva) from the transparent cornea. It is a region of interest because it is the site of numerous biological activities ranging from blood supply of the cornea within the anterior eye, to housing the aqueous outflow apparatus. While the former is important for nutrition and waste removal purposes, the latter is significant for the proper maintenance of intra ocular pressure (IOP). An alteration in limbal architecture can lead to increased IOP and result in blinding disorders such as glaucoma. Perhaps an in vivo, non-invasive and non-contact means of monitoring and measuring the structures within the limbus at an ultra-high resolution would be beneficial as an aid to diagnosis and evaluation of anterior ocular conditions involving the various components of the limbus.

During both awake and asleep conditions, the superior limbus is covered by the upper eyelid; in fact, it conceals roughly two millimeters of the superior corneal region (the total area of the superior limbus), while the eye is in the open-eye primary-gaze position (Oyster, 1999). This causes a barrier to oxygen uptake within the limbal zone. Studies seem to demonstrate that immediately after the retraction of the upper eyelid, superior corneal oxygen uptake is much higher than other parts of the cornea (W. Benjamin & Hill, 1988; W. Benjamin & Rasmussen, 1988; Fitzgerald & Efron, 1986) but when the whole cornea including the superior region is exposed to unvarying oxygen conditions through the retraction of the upper

eyelid, there is no difference in oxygen uptake of the various regions (W. J. Benjamin & Ruben, 1995). When oxygen delivery to the limbus is reduced, limbal hyperemia occurs as blood flow is increased to the region (E. Papas, 1998; E. B. Papas, Vajdic, Austen, & Holden, 1997). Since normal limbal vessels are not always in a state of hyperemia it can be expected that anatomical and physiological alterations within the tissue might occur as a response to overcome the possible inadequate exposure to atmospheric oxygen that the superior limbus experiences as a result of it being constantly covered by the upper eyelid. Such adjustments in response to this chronic hypoxia might include but are not limited to, changes in vessel size, density and depth, as well as changes in epithelial thickness. Previous studies have revealed differences in the density of endothelial cells (Amann, Holley, Lee, & Edelhauser, 2003), diameters and spacing of collagen fibrils (Boote, Dennis, Newton, Puri, & Meek, 2003), stem cell size (Romano et al., 2003) and the thickness of the cornea (Liu, Huang, & Pflugfelder, 1999; Liu, Xie, & Zhang, 2001; Remon et al., 1992) between the superior limbus and other positions of the corneal limbus. It is important to note that only a few human morphometric studies involving high resolution non-contact devices dedicated to the superior limbal region have been carried out (Bizheva, Hutchings, Sorbara, Moayed, & Simpson, 2011; Simpson, Bizheva, Feng, Alabi, & Hutchings, 2012).

1.2 Purpose of the study

To compare and investigate morphometric characteristics of limbal vasculature within the superior and inferior limbal regions using ultra-high resolution optical coherence tomography.

1.3 Research questions

By completion of this study the following research questions will be adequately addressed.

1. Is the UHR-OCT capable of imaging and measuring characteristics of size and depth of vessels within the limbus in a repeatable manner?
2. Is there a difference in the size of vessels across different positions of the limbus?
3. How deep are the vessels found within the limbus?

Chapter 2

2.0 Literature overview

2.1.1 Anatomy of the limbus

The limbus is a region of transition within the anterior portion of the eye that possesses both structural and physiological importance. Essentially this area, about 1.5mm wide horizontally and 2mm wide vertically, spans circumferentially around the iris and is the zone that encompasses parts of the peripheral cornea, bulbar conjunctiva, and sclera (Van Buskirk, 1989). The limbus is important as it contains the aqueous humour pathways and is partly responsible for nourishing the cornea. It is also the location for incisions during surgical procedures to address glaucoma, cataract and other anterior segment complications, and provides structural support for the cornea by anchoring corneal fibers (Hogan, Alvarado, & Weddell, 1971; Van Buskirk, 1989).

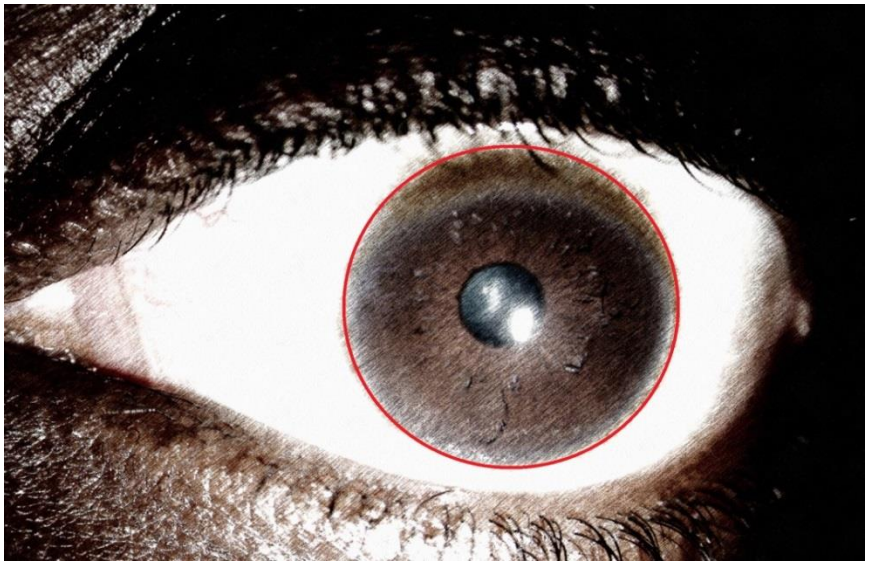

Figure 1: Enface outline of the human limbus.

2.1.2 Macro structure

What defines the limbus is quite varied depending on the background of the professional investigating this zone. For example the ocularist, one who fabricates ocular prosthesis (Jahrling, 1999), may define the limbus as the pigmented circular edge around the iris and will only use color discrepancy as a means of differentiation. The histologist might define the limbus based on microscopic tissue and cell structure and morphology. Since scleral collagen tends to be more eosinophilic and their fibers larger (700 – 1000A) than corneal collagen fibers which are generally less than 600 A in diameter (Han, Giese, & Bille, 2005), it may form a basis for defining the limbus for a histologist. The pathologist would further define the limbus based on anatomical landmarks where the termination of the Bowman's membrane and Descemet's layer at the peripheral cornea would be the anterior border of the limbus. The posterior limit of the limbus has been defined in this way by a plane from the scleral spur orthogonal to eyeball surface (Van Buskirk, 1989).

For the purposes of this study the limbus was defined as the area that falls within the corneo-limbal and sclero-limbal boundaries. From Figure 2, the transitional area of the limbus is clearly visible and the corneo-limbal can be defined by an imaginary line from the edge of the perceived termination of the Bowman's membrane to the termination of Descemet's membrane. On the other hand, the sclera-limbal boundary can be defined as an orthogonal line from the ocular surface passing through the furthermost insertion of the sclera into the anterior chamber.

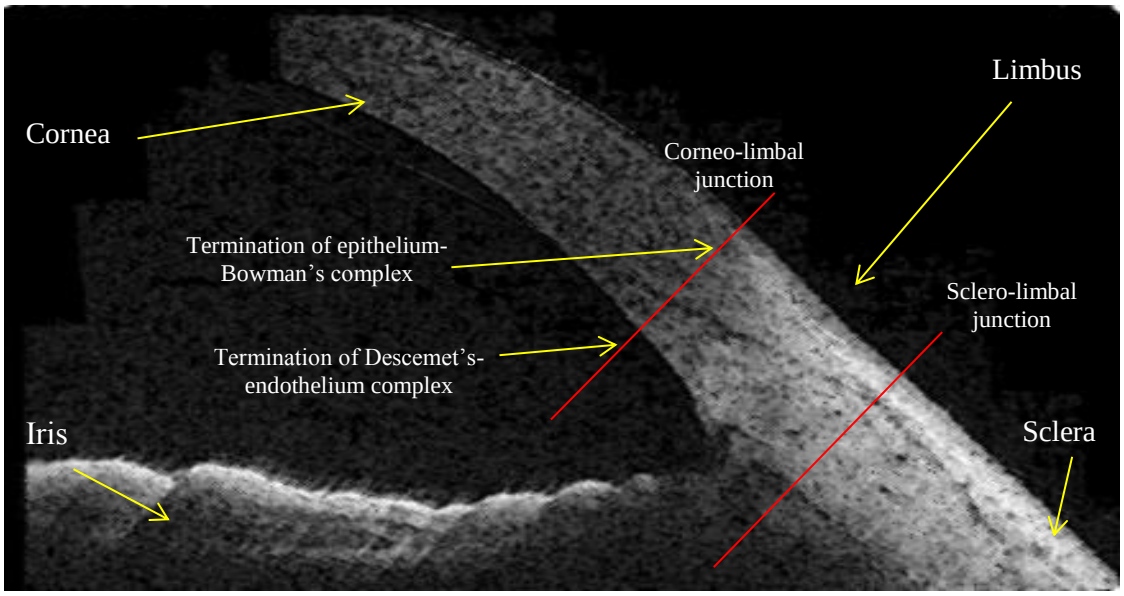

Figure 2: Defining the location of the limbus in an OCT tomogram. For the purposes of the studies described in this thesis, the limbus is the transitional region between the corneo-limbal junction and the sclero-limbal junction.

The superior and inferior regions of the limbus possess a greater extension of the sclera than the nasal and temporal portions and this may account for the rather elliptical shape of the corneo-scleral junction (Hogan et al., 1971). Conjunctiva terminating at the periphery of the Bowman's membrane overlies the external limbal surface and spike-like radiations within this peripheral corneal area, known as Vogt's palisades, are found in the corneal epithelium protruding into the limbus (Oyster, 1999). Conjunctival stromal papillae and epithelial rete pegs are responsible for the formation of these palisades and they are found more in the superior and inferior regions of the limbus and measure about 500 microns in width (Townsend, 1991). Individuals of darker complexion have more prominent palisades as a result of heavy pigmentation (Khan, Niazi, & Awan, 2012).

2.2 Epithelium across the limbus

2.2.1 Corneal epithelium

The corneal epithelium here consists of non-keratinized, stratified squamous cells and its 4-7 cell layers are roughly 50 micrometers thick. This thickness is more or less regular across the whole cornea (Farjo, McDermott, & Soong, 2009). A tear film covers the epithelium and this is significant as it eliminates irregularities in the anterior epithelial layer and contributes to the refractive capabilities of the cornea. The superficial epithelial cells are flat, polygonal in shape, and about 2-3 cell layers thick.

Beneath the surface epithelial cells are the wing cells. These cells also known as supra-basal cells are about 2- 3 layers thick but differ from the superficial cells by being less flat. Beneath the wing cells is the basal layer which is only one layer thick and forms the deepest cellular layer of the corneal epithelium making up about 40 percent of the epithelium. With the exception of transient amplifying cells and stem cells, basal cells are the only other epithelial cells of the cornea that are capable of mitosis. The corneal epithelium is unique as it is specialized to overlay avascular connective tissue. The epithelial cells have a turnover lifespan rate of about 5 – 10 days (Hanna, Bicknell, & O'Brien, 1961).

2.2.2 Limbal epithelium

While the structure of the limbal epithelium appears to be similar to that of the corneal epithelium, there are some major differences between the limbal and corneal epithelium. Firstly, there appears to be frequent intermixing of melanocytes between cells of the limbal epithelium (Hogan et al., 1971). Also, the basal cells of the limbal epithelium possess a

smaller number of hemi-desmosomes and this causes undulating extensions of the basal cell surface into the matrix below. It is believed that this undulation provides an increased surface area for the basal cells which facilitates the taking up of nutrients from the limbal vasculature (Hogan et al., 1971). Finally, the limbal basal cells tend to be smaller, less columnar in shape and have been reported to possess more mitochondria than corneal basal cells (Gipson, 1989).

2.3 Limbal vasculature

The main blood delivery to the eye originates from the ophthalmic artery, this then yields two distinct yet related branches, one being located deeper while the other more superficially. The superficial circulatory component eventually forms the episcleral arterial circle but prior to this, supplies the rectus muscles by way of the anterior ciliary artery. The deeper circulatory component of the ophthalmic artery, the intra-ocular arterial circle, passes anteriorly through the sclera, enters the major circle of the iris and supplies both the ciliary body and iris (Meyer, 1989). Figure 3 illustrates the arrangement of vessels present within the limbal region of the eye.

2.3.1 Conjunctival vasculature

Capillaries and post capillary venules constitute the bulk of vessels observed in the conjunctiva. The vessels towards the corneo-limbal portion of the limbus have less fenestrations and a thicker endothelium as compared to the vessels in the conjunctiva towards the sclera-limbal junction (Iwamoto & Smelser, 1965). Arterioles, which constitute the majority of arterial blood supply in the conjunctiva of the limbus, form an intricate sub-

conjunctival network of capillaries (Fawcett, 1963). The superficial perilimbal plexus encompass the cornea providing branches that nourish the peripheral cornea. These branches travel onward into the Vogt's palisades' papillae where they are further broken down into two sets of vessels, one set which forms the arcades of the peripheral cornea and then become venous (perilimbal venous plexus), and branches of the circular limbal artery that are recurrent and supply both the peripheral cornea and perilimbal conjunctiva (Morrison & Van Buskirk, 1983).

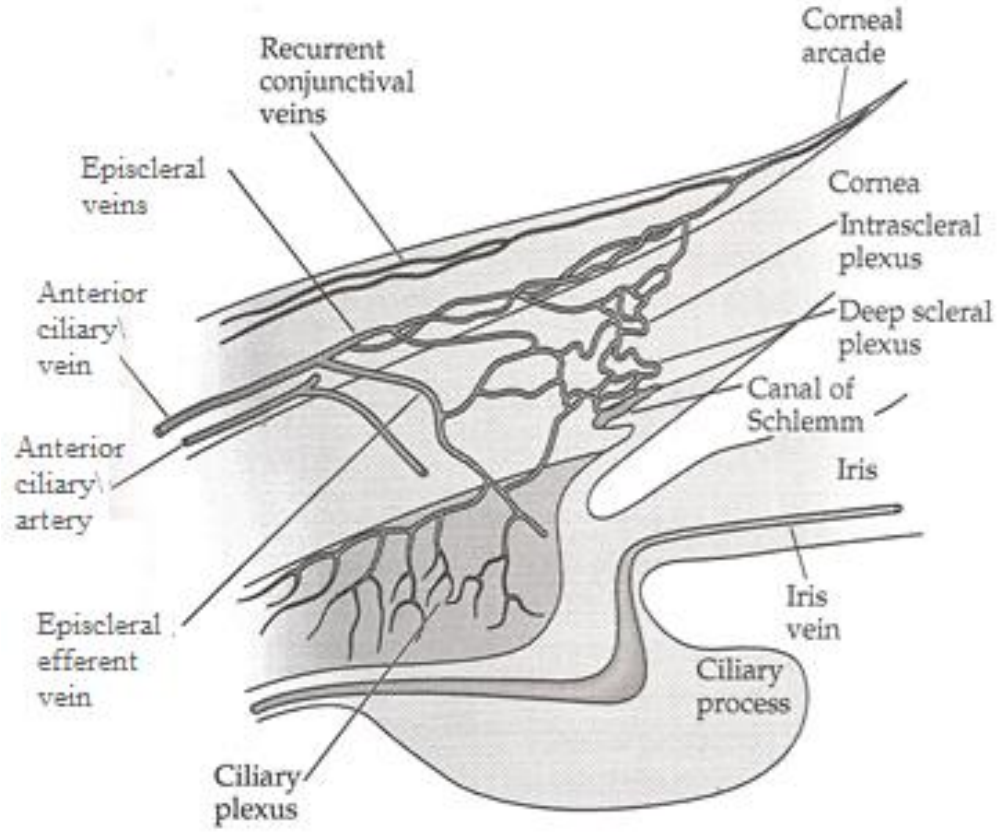

Figure 3: The limbal vasculature. An illustration of the major arteries and veins that can be found within the corneo-scleral limbus. Reproduced with permission from Sinauer Associates, Inc.

2.3.2 Episcleral and scleral vasculature

The arterial vessels within the episclera arise from branches of the circular limbal artery and anterior ciliary artery. They provide nourishment for the sub-conjunctival tissues and merge with the superficial vessels of the conjunctiva (Ashton, 1951a). The arterial flow within the sclera is supplied directly by the main trunk of the anterior ciliary arteries and its branches travel through the sclera to merge with the major circle of the iris (Dvorak-Theobald, 1934).

2.3.3 Venous outflow

Posterior to the limbal arcades is a circular system of vessels, the limbal venous circle, through which blood exits the limbus. A collection of radial veins within the episclera carry the blood from the venous circle backwards, toward the recti muscles. This is the exit route for blood within the anterior conjunctiva, episclera and also Tenon's capsule (Fawcett, 1963). An interconnecting venous network within the sclera known as the intra-scleral plexus receives blood from the ciliary plexus and the deep scleral plexus, the latter can be found lying within proximity to the Schlemm's canal. The intra-scleral and deep scleral venous plexuses drain posteriorly into the episcleral venous plexus.

2.4 Blood flow and regulation in the limbus

The limbal vessels form part of a greater vascular network where metabolic waste and nutrient transfer between tissue and blood takes place; this microcirculation system is cardinal to the proper functioning of all cells in the body (van der Merwe & Kidson, 2010). It is evident that a rather powerful pump and a great volume of blood would be required for constant perfusion of this large network of blood vessels, yet the body adopts a local

approach in altering the blood flow to cater for the needs of specific tissues (Kaufman, Levin, Alm, Nilsson, & Ver Hoeve, 2011). The body in general regulates blood flow to local tissues via mechanisms such as myogenic control, sympathetic and parasympathetic innervations to smooth muscle, metabolic activity within the parenchymal cells surrounding the blood vessels of interest, and finally humoral elements intrinsic in blood that have the capacity to alter smooth muscle cells of blood vessels (Furness, 1973; Furness & Marshall, 1974; Wiedeman, 1968). Examples of these factors include epinephrine, serotonin, histamine, angiotensin and vasopressin (Schmetterer & Kiel, 2009). These general mechanisms highlighted above depend on the capability of smooth muscle within blood vessels to effect changes on vessel calibre, but it is clear that blood flow in the limbus stems from a capillary network where smooth muscle is absent (Lepple-Wienhues, Stahl, & Wiederholt, 1991).

A possible mechanism through which the limbal capillaries control blood flow is via the last smooth muscle cell found most peripheral along any terminating arteriole branch, the pre-capillary sphincter (Bloch, 1956). This sphincter can be envisioned as a door that opens up to allow perfusion of blood to the distal capillary bed or, closes to impose a shutdown of blood flow (Granger, Schelling, Lewis, Zawieja, & Meininger, 1988). It is important to note that while some capillaries are filled with blood, others are not, as the pre-capillary sphincter opens and closes in a selective manner (Oyster, 1999). Also, blood flow within the capillaries is not always in one direction neither is it continuous (Granger, Borders, Meininger, Goodman, & Barnes, 1983).

Another mechanism for the control of limbal vessel perfusion depends on capillary contractility. Although capillaries cannot contract primarily due to the absence of smooth

muscles, some authors have shown the contraction of endothelial cells within capillaries (Aharinejad et al., 1993; Ragan, Schmidt, MacDonald, & Groom, 1988). An attempt to explain this capillary contractility highlighted the possible involvement of pericytes (Fawcett, 1963). In as much as the controversy over capillary contractility continues, it is apparent that the probable occurrence of pericyte contractility makes local perfusion of blood capillaries within the limbus more feasible (E. B. Papas, 2003).

2.4.1 Nerves of the limbus

Branches of the fifth cranial nerve pass through the limbus and terminate in the cornea (Müller, Marfurt, Kruse, & Tervo, 2003). Its distribution is through the long posterior ciliary nerves which supply majority of the limbal region including the trabecular meshwork and Schlemm's canal and extends to innervate the cornea (Al-Aqaba, Fares, Suleman, Lowe, & Dua, 2010). Nerves within the limbal stroma contain both myelinated and unmyelinated branches while greater portion of these nerves tend to be sensory in nature (Marfurt, Cox, Deek, & Dvorscak, 2010).

2.5 Visualization of the limbal region

Many methods exist for the visualization and morphometric analysis of structures within the limbus. Ex-vivo technology such as serial histologic sections (Dvorak-Theobald, 1934; Hamanaka, Bill, Ichinohasama, & Ishida, 1992; Krohn & Bertelsen, 1998) and ultrathin sections (Bron, 1997; Smith et al., 2000) have been used to visualize ocular vessels, trabecular meshwork and aqueous outflow in the limbus. Some shortcomings associated with histological sectioning is that the curvature of the eye provides a barrier to the reconstruction

of anatomical structures including vasculature, from sectioned materials and the process cannot be carried out in vivo (Burger, Chandler, Fryczkowski, & Klintworth, 1987).

In vivo methods of visualizing the limbus include but are not limited to slit lamp microscopy (SLB), gonioscopy, confocal microscopy, ultrasound biomicroscopy (UBM) and optical coherence tomography (OCT).

2.5.1 SLB and gonioscopy

In ophthalmic practice, slit lamp biomicroscopy is one of the techniques to observe the anterior eye (Turtz & Fisher, 1979). SLB has been used in the detection and morphological study of aqueous veins and aqueous outflow mechanisms (Ascher, 1953). Limitations to using this method of imaging include the rather poor resolution, such that the origin of aqueous veins at the intra-scleral plexus, trabecular meshwork and Schlemm's canal is not identifiable (Ascher, 1953).

With the aid of a gonio-lens the observer can visualize the irido-corneal angle as well as the inside of the anterior chamber and while some investigators have been able to identify the Schlemm's canal, they are quick to admit that the visualization is best when the canal is filled with blood (Kronfeld, 1948; Kronfeld, 1949; Moses, Hoover, & Oostwouder, 1979; Turtz & Fisher, 1979).

2.5.2 Confocal microscopy

In 1955 Marvin Minsky invented confocal microscopy and it was used to study neural networks within the brain (Petroll, Jester, & Cavanagh, 1994). In vivo confocal microscopy has been previously applied to examine different parts of the cornea (Patel & McGhee,

2007). Some advantages associated with confocal microscopy include its minimally invasive to non-invasive approach and superior lateral resolution of approximately 0.6 – 1um/pixel which permit visualization of structures at the cellular level (Pawley, 1995; Pawley, 2006). Depending on the type of confocal microscope, the scan acquisition time is rapid at about 27 frames per second (Niederer & McGhee, 2010). Some disadvantages associated with confocal microscopy include relatively limited penetration depth in scattering tissue (< 500um), as compared to OCT, and its contact approach (Pawley, 2006), as well as a limited field of view which is as a result of the high optical resolution as magnification is inversely proportional to the field of view (Cox & Sheppard, 2004).

2.5.3 Ultrasound biomicroscopy (UBM)

The utilization of high frequency ultrasound to image biological tissue at a microscopic resolution is termed UBM, this technology was applied in the early 1990's (Allemann et al., 1993; C. Pavlin, Harasiewicz, Sherar, & Foster, 1991; C. J. Pavlin, Sherar, & Foster, 1990; Reinstein, Silverman, Trokel, & Coleman, 1994; Reinstein, Silverman, Rondeau, & Coleman, 1994) and has been applied to various ocular structures including the cornea, ciliary body, iris, anterior chamber angle and zonules (Foster, Pavlin, Harasiewicz, Christopher, & Turnbull, 2000; C. J. Pavlin & Foster, 1995; C. J. Pavlin et al., 1990; C. J. Pavlin & Foster, 1998). Strengths of high frequency UBM include a fairly good axial and transverse resolution of about 25um and 50um respectively. Another major strength of UBM is its ability to image through opaque media; it possesses about 5mm of depth penetration in tissue (Ishikawa & Schuman, 2004). UBM requires probe contact and water bath immersion

which tends to be time demanding, requires high examiner skill and tends to cause artifacts in anterior angle measurements (Ishikawa, Inazumi, Liebmann, & Ritch, 2000).

2.6 Optical coherence tomography (OCT)

2.6.1 Introduction and definition of OCT

OCT is a non-invasive optical imaging method that provides high resolution cross–sectional images of optically scattering media (Huang et al., 1991). In order to investigate the depth of a target structure using OCT, the round trip delay time of a reflected wave is used; this in some ways makes it analogous to ultrasound imaging (Clivaz, Marquis-Weible, Salathe, & Gilgen, 1992). The major difference of utilizing light instead of acoustics gives OCT the ability to provide a higher resolution due to the shorter wavelength (Huang et al., 1991) and faster acquisition times (Huang et al., 1991; Simpson & Fonn, 2008) since light travels at a greater speed than sound (Ockert, 1968).

A quick search was performed in "Scopus", a science research database, for an idea on the relative expansion of OCT research. This was done by searching for articles, papers and reports that had "Optical Coherence Tomography" in its title, abstract or used as keywords. The results of this search indicating the number of publications found per year are displayed in Figure 4.

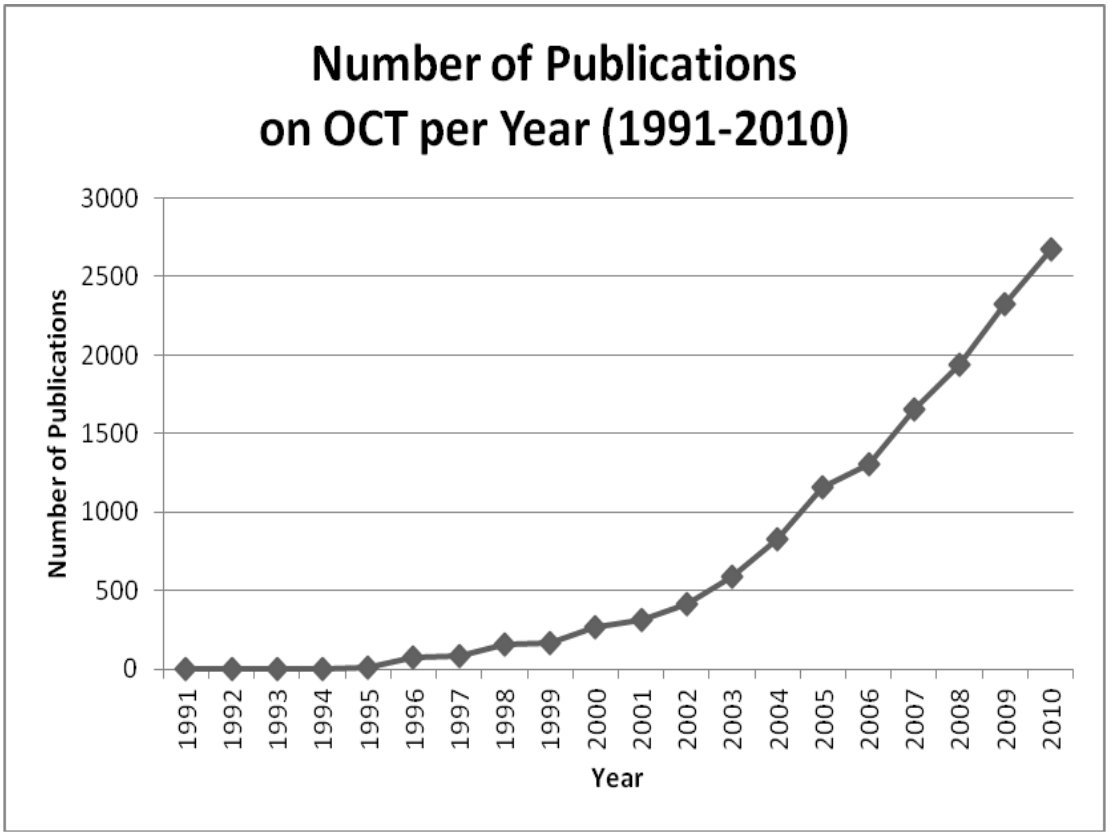

Figure 4: Number of articles found using Scopus research database with "optical coherence tomography" as part of the publication title, abstract or keyword.

2.6.2 Origin of OCT

OCT emerged from in vivo optical length measurements of the eye via white light interferometry ((Fercher, Mengedoht et al. 1988; Fercher, Hitzenberger, Kamp, & Elzaiat, 1995). Applications in fiber optics and integrated-optic structures initially utilized optical coherence domain reflectometry**;** this technology was subsequently applied to biological structures including the eye (Fercher, Mengedoht, & Werner, 1988; Fercher et al., 1995) and

blood vessels (Clivaz, Marquis-Weible, Salathe, & Gilgen, 1992; Swanson et al., 1993). In 1991, OCT was reported for the first time by David Huang and partners at the Massachusetts Institute of Technology (Huang et al., 1991).

2.6.3 Types of OCT

In terms of optical design, OCT can be classified into two broad groups, time domain OCT (TD OCT) and Fourier domain OCT (FD OCT). The principle of operation of OCT is based on low coherence interferometry (Fercher et al., 1995). With regards to OCT technology applied in ophthalmology, light reflected from different positions within the eye, interferes with light that has travelled a known path length that is reflected from a stationary (FD OCT) or moving (TD OCT) retro-reflector or mirror.

2.6.4 Time domain OCT

Time domain OCT makes use of reflections from within tissues to provide cross-sectional images (Huang et al., 1991). In this type of OCT, the period of light delay for light reflected off a tissue of interest is compared with, the period of light delay from a scanning (moving) reference mirror at a known distance (Ramos, Li, & Huang, 2009; Sakata, DeLeon-Ortega, Sakata, & Girkin, 2009). From this comparison, a reflectivity profile displaying spatial dimension and structure location information within the tissue in the form of axial scans (A scans) is formed. These A scans are then further combined to form a cross-sectional tomography (Sakata, DeLeon-Ortega, Sakata, & Girkin, 2009).

Examples of TD OCT applied to anterior segment imaging include the slit-lamp OCT (Heidelberg Engineering GmbH, Heidelberg, Germany) and the Visante OCT (Carl Zeiss

Meditec, OH, USA) operating at longer wavelengths of 1310 nm range and providing a transverse optical resolution of about 60 – 100 micrometers (Konstantopoulos, Hossain, & Anderson, 2007).

The utilization of a longer wavelength in these designs theoretically permits greater penetration of highly scattering anterior segment tissue though this occurs with an associated loss in resolution. When longer wavelengths are employed, less scattering within opaque tissues such as the sclera and iris occurs as interpreted from the Rayleigh Principle for scattering by small particles. The Rayleigh Principle states that the strength of scattering is inversely proportional to the fourth power of the wavelength (Hulst, 1957).

2.6.5 Fourier domain OCT

The second broad group of OCT devices, Fourier domain OCT, operates by acquiring broadband interference with detectors that are spectrally separated (Choma, Sarunic, Yang, & Izatt, 2003). In this type of OCT, the reference mirror is stationary, unlike that of TD OCT where the reference mirror is always in motion during the acquisition process (Fercher et al., 1995). Reflections emanating from all layers in the tissue of interest are simultaneously detected and the lack of moving elements allow for rapid image acquisition and a greater signal to noise ratio (Choma, Sarunic, Yang, & Izatt, 2003; de Boer et al., 2003; Leitgeb, Hitzenberger, & Fercher, 2003; Schmitt, 1999).

2.6.6 Spectral domain OCT (SD OCT)

In spectral domain OCT, a dispersive element or spectrometer is employed to distribute varying optical frequencies onto a light detector stripe, this is usually an array of charged

couple devices (CCDs) or complimentary metal-oxide semi-conductors (CMOS), to extract spectral information. A set of mathematical calculations involving Fourier relations is then employed to acquire depth information (van Velthoven, Faber, Verbraak, van Leeuwen, & de Smet, 2007). A clear distinction lies in the overall performance of SD OCT as compared to TD OCT as the former possesses enhanced image acquisition speed since optical scanning is faster than mechanical scanning (Fujimoto, Jim 2006).

SD OCT devices with an axial resolution of about 2 – 3 micrometers with image acquisition speeds of about 47,000 axial scans per second have been employed in many studies to image the anterior portions of the eye including the upper eyelid (Bizheva, Lee, Sorbara, Hutchings, & Simpson, 2010), cornea (Hutchings et al., 2010) and limbus with a great amount of success (Bizheva et al., 2011; Simpson et al., 2012).

2.6.7 Swept source OCT (SS OCT)

Swept source OCT devices operate by sweeping a narrow line width tunable laser through a broad optical bandwidth and time encoding the spectral information gathered (M. A. Choma, Hsu, & Izatt, 2005). A single photodiode detector is used in SS OCT just as in TD OCT, though some SS OCT devices utilize a dual balanced detector (Fujimoto, 2006).

Applications of SS OCT to the anterior segment range from imaging corneal thickness (Neri et al., 2012) and topography (Karnowski, Kaluzny, Szkulmowski, Gora, & Wojtkowski, 2011) visualization of Schlemm's canal (Shi et al., 2012) and anterior chamber angle (Grulkowski et al., 2012).

Chapter 3

Materials and methods

3.1 Optical coherence tomographic imaging

A high speed spectral domain UHR-OCT system operating at ~1060nm (Figures 5 and 6) was developed in our lab for in vivo imaging of the human anterior chamber and applied in a study of hypoxia-induced corneal swelling in humans (Hutchings et al., 2010). The UHR-OCT system and imaging interface provide ~3μm axial and ~18μm lateral resolution in biological tissue and depth of focus of ~250 μm (Rayleigh range). The UHR-OCT system also provides ~92dB SNR for 1.4mW power of the imaging beam (Hutchings, Hyun, Bizheva, & Simpson, 2010). When applied to imaging the anterior structures of the human eye, an UHR-OCT system operating in the 1060nm spectral range has a major advantage over similar systems operating at 800nm or 1300nm; the dispersion of water has a null at ~ 1060nm and provided that the optical dispersion within the UHR-OCT imaging system is balanced, the images acquired do not require post-processing for water dispersion compensation (Bizheva et al., 2011). Also, devices operating at the 1060nm range are more suited for imaging anterior eye segment structures as they provide greater depth penetration in highly scattering biological tissue such as the limbus, sclera, eyelid, etc., as compared to devices operating in the 800nm range (Bizheva et al., 2011; Steinert & Huang, 2008). Figure 5 illustrates the different components of the UHR-OCT system used for acquisition of all data presented in this thesis.

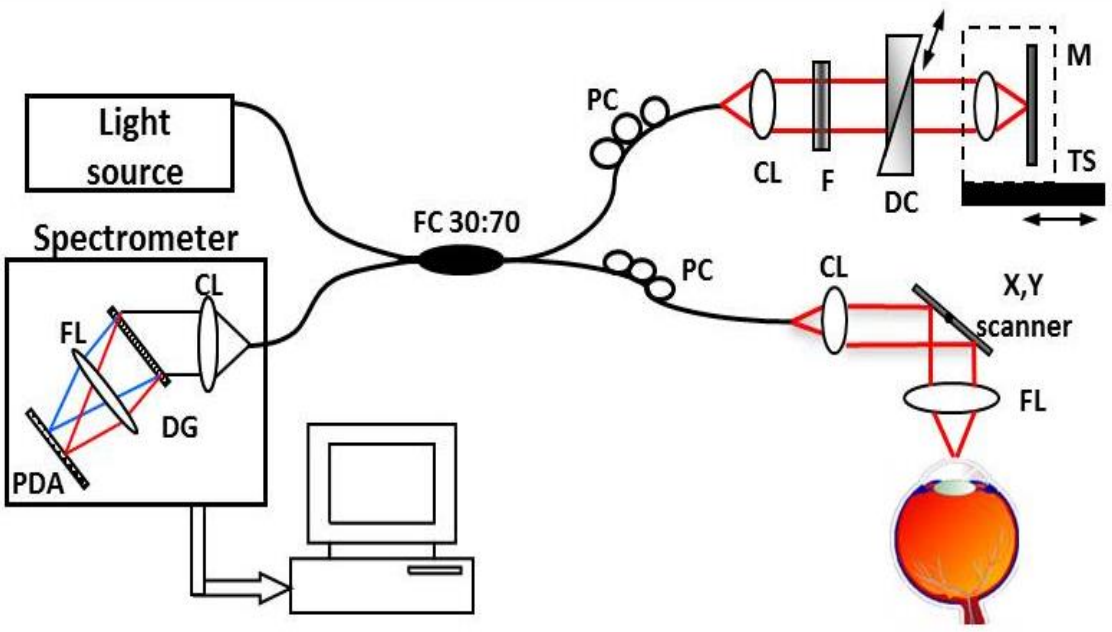

Figure 5: Schematic representation of spectral domain UHR-OCT device. PDA – photo detector array (CCD camera), FL – focusing lens, DG – diffracting grating, CL – collimating lens, FC – fiber coupler, PC - polarization controller, F – filter, DC –dispersion compensation, TS – translation stage, M – mirror.

3.1.1 UHR-OCT calibration

Details about the calibration of the OCT used in acquiring data for this research are described in Hutchings et al, 2010 (Hutchings et al., 2010). Briefly, in order to ascertain that an optical device such as the UHR-OCT is truly quantifying physical thickness the application of an in vivo procedure for taking optical measurements of distance within an item of interest that utilizes the approximation of refractive index and identified values of ex vivo thickness can be employed. Measurements of thickness of a phantom whose refractive index (1.376 + 0.0005 @ 589nm; Optical Polymer Research Inc., Gainesville, FL, USA) and physical

thickness values (104–764µm measured using a precision mechanical gauge; Vigor GA-715, Japan) are known were obtained and compared with the UHR-OCT device. From the results it was concluded that the UHR-OCT device was accurate, repeatable and capable of human corneal morphometry (Hutchings et al., 2010). For the application of the UHR-OCT system to imaging in the corneo-limbal region, it is important to note that there is a possible variation in refractive index in the zone where the cornea transitions into sclera as axial and lateral local variations in the refractive index of bovine and human corneas have previously been demonstrated (Vasudevan, Simpson et al. 2008). For further measurements of vessel depth and vessel size in this thesis, an average refractive index of 1.376 was assumed for the corneo-limbal region.

Figure 6: Spectral domain UHR-OCT device set up.

3.2 Participants

Fourteen healthy participants were involved in the study. All subjects met the inclusion criteria and did not demonstrate any of the exclusion criteria, itemized below. Experimentation was carried out on the subjects after noon to eliminate any influence of diurnal variation (Feng, Varikooty, & Simpson, 2001).

3.2.1 Inclusion and exclusion criteria

The participant qualified for entry into the study if he or she:

1. Was between the ages of 16 to 60 years.

2. Understood and signed an informed consent statement.

3. Was a non-contact lens wearer.

Subjects were excluded if he or she,

1. Had any systemic disease that affected ocular health.

2. Had any ocular disease.

3. Had a history of ocular surgery.

4. Had a refractive error $\leq \pm 4$ D and astigmatism ≤ 2 D.

3.3 Study procedures

Four phases were required for this experiment; a summary of these stages is illustrated in Figures 7 and 8.

3.3.1 Phase one - screening procedure

Potential volunteers for this study were evaluated for eligibility using standard clinical techniques of visual acuity, case history, slit lamp biomicroscopy (including use of fluorescein sodium dye to assess the integrity of the surface of the cornea) and assessment of their current corrective device. Participants were asked if they had had recent eye examinations (within the last two years) and active ocular conditions other than refractive error. In cases where the screening procedures contraindicated participation in the study (examples being hyperemia, dryness, corneal compromise, observed corneal disease or problems with vision), the participant was not recruited for further participation.

3.3.2 Phase two - pre-test procedure

The imaging procedure was explained in detail to them by the principal investigator and all questions regarding the imaging procedure and safety concerns were answered. Participants who wished to take part in the study then read the information letter and signed the consent form.

3.3.3 Phase three - imaging procedure

Imaging with the UHR-OCT device was carried out on the participants after manual retraction of their upper or lower eyelids whiles they were fixated on a target inferiorly and superiorly, respectively. When the subject looked inferiorly the superior limbus was imaged and vice versa. Head position remained approximately fixed as the subject was comfortably positioned in a chin and forehead rest. This helped to minimize image artifacts arising from head motion.

Eye and OCT position was coordinated to align the probe approximately perpendicular to the ocular surface. At the limbus (with the smallest scan length) when the incident light was at a right angles to the ocular surface, the OCT image appeared horizontal and a specular reflection (from, primarily, the most anterior limbal surface/tear layer) was present at the centre of the image. The optical beam was raster scanned over the imaging area.

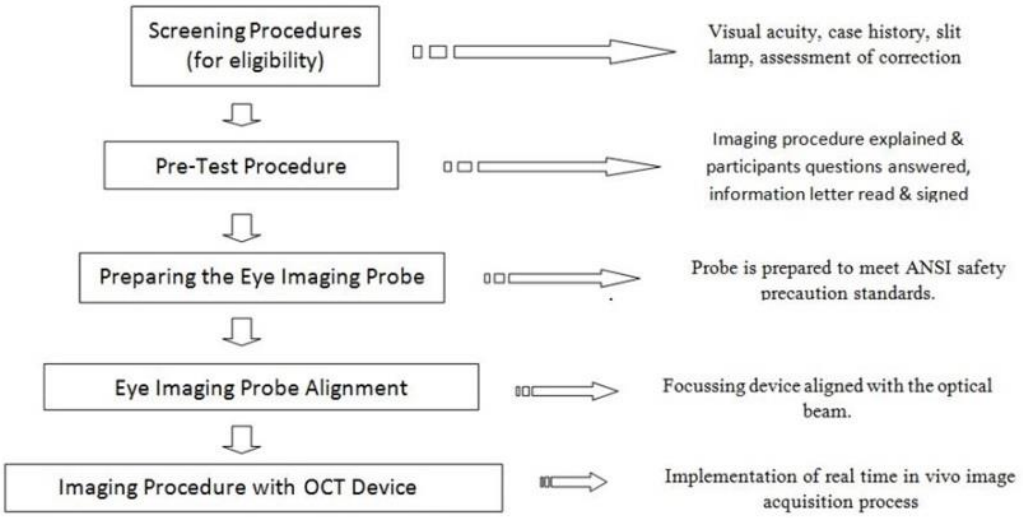

Figure 7: A summary of the data acquisition process.

3.3.4 Phase four - data processing and analysis

All tomograms were processed with Matlab (Mathworks), Amira (Visage Imaging) and Image J (National Institute of Health). 8 bit image stacks (1000 x 1024 x 256) were acquired of the transition from clear cornea to bulbar conjunctiva at the superior and inferior limbal region. To define the limbal region, an imaginary orthogonal line was drawn from the termination of the Bowman's-epithelium complex through the termination of the endothelium-Decemet's complex (Figure 2). This denoted the corneo-limbal junction, while

an imaginary line orthogonal to the ocular surface though the furthermost insertion of the sclera to the anterior chamber denoted the sclera-limbal junction (Figure 8). The area that fell within these two borders was presumed to be the limbal zone.

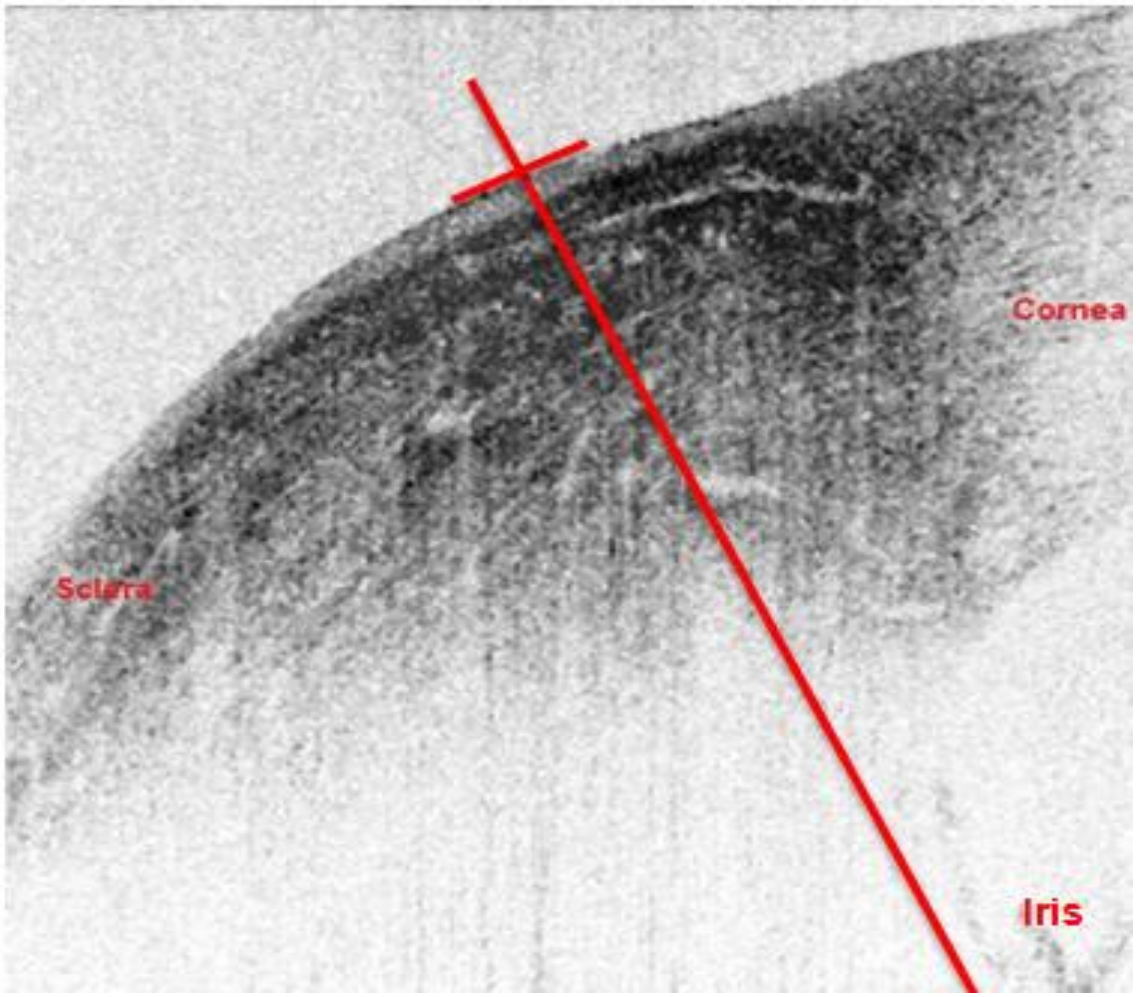

Figure 8: Identifying the sclero-limbal junction in an UHR-OCT tomogram of the limbus. The line displays the approximate Sclero-limbal border.

Prior to analysis, all the images were processed with band pass filter (small structures up to 2 pixels) to enhance the visualization of edges within the image (Schneider, Rasband, & Eliceiri, 2012). Finally, for the purposes of investigating vessel size, individual sets of images were registered into a 3D stack and alignment was accomplished using a standard translation transformation (Thevenaz, Ruttimann, & Unser, 1998).

After a three dimensional reconstruction, the diameters of all clearly visible vessels within the limbal region were measured using a circle or ellipse tool (the shorter diameter in case of an ellipse tool), as required, this represented vessel size. The vessel depth was quantified as the distance from the anterior most ocular surface to the outer most boundaries of all observable vessels.

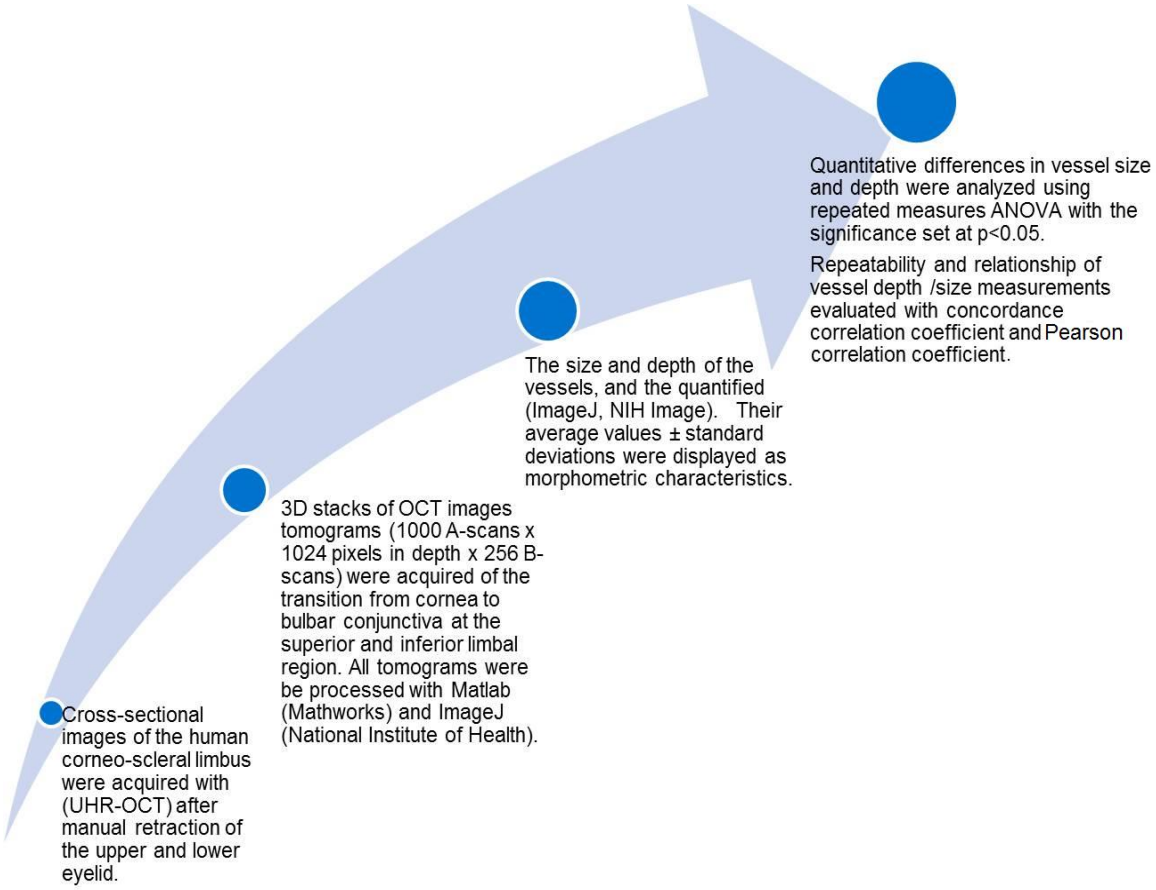

Figure 9: A summary of the data processing and analysis procedures.

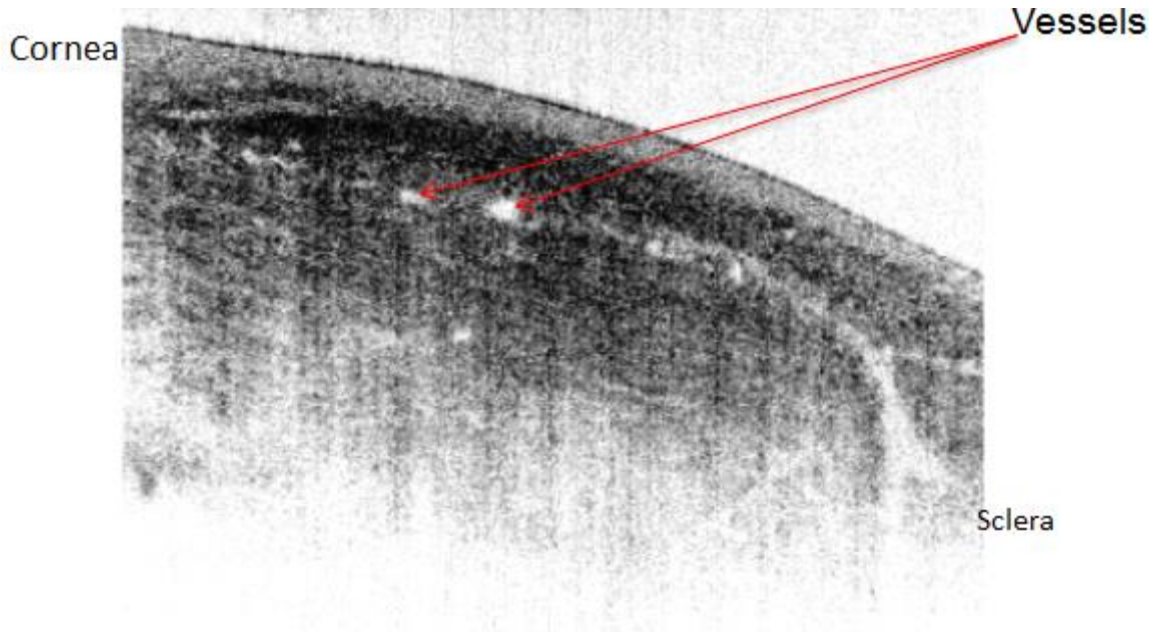

Figure 10: UHR-OCT tomogram of the limbal region showing vessels. The arrows represent vessels which appear as lower scattering circular areas within the limbal regions, their diameters representing vessel size were measured.

Vessel depth and size measurements were repeated for the same vessel and the concordance correlation coefficient was computed to assess the agreement between the repeated measures. Pearson correlation coefficients were calculated to investigate the linear relationship between vessel size and depth within the superior and inferior limbus. Quantitative differences in vessel size and depth in the limbal region were analyzed using repeated measured ANOVA. R and SPSS were used for all data analysis procedures while morphometric characteristics were tabulated with Microsoft Excel.

Chapter 4
Results

The morphometric characteristics of vessel size and depth of 14 randomly selected eyes were measured on 14 subjects, a summary for these characteristics can be found in Tables 1 and 2.

Table 3: Morphometric characteristics for the superior limbal region.

Subject	**Vessel Size(μm)**		**Vessel Depth(μm)**		**# of Vessels**
	Mean Value ± SD	**Min – Max Values**	**Mean Value ± SD**	**Min – Max Values**	
1	29.845 ± 17.339	13 - 74.982	134.205 ± 100.054	51.518 - 421.101	18
2	32.794 ± 22.438	13 - 82.14	180.206 ± 111.813	49.583 - 362.81	10
3	23.771 ± 11.926	12.3 - 55.318	117.083 ± 79.674	52.065 - 298.708	12
4	31.993 ± 24.236	12.39 - 82.73	149.386 ± 80.397	67.6 - 285.386	9
5	31.262 ± 16.135	17.87 - 62.81	224.982 ± 39.534	173.252 - 293.453	6
6	32.635 ± 25.781	12.06 - 81.903	151.71 ± 92.427	61.883 - 311.33	9
7	30.322 ± 15.011	21.06 - 63.025	207.347 ± 85.894	101.433 - 339.342	7
8	30.588 ± 16.209	15.094 - 71.5	217.816 ± 164.641	84.601 - 684.136	11
9	32.062 ± 19.310	19.67- 71.54	243.506 ± 125.176	126.261 - 467.004	9
10	31.283 ± 20.148	7.425 - 63.335	193.477 ± 147.228	65.130 - 542.257	10
11	17.193 ± 7.736	7.8 - 31.504	114.003 ± 57.554	48.170 - 213.30	8
12	24.595 ± 13.885	8.01 - 55.375	165.287 ± 108.754	68.087 - 400.778	8
13	31.306 ± 15.126	18.04 - 57.06	237.009 ± 118.159	62.589 - 519.924	10
14	29.294 ± 18.732	11.714 - 77.620	197.648± 52.378	93.832 - 315.441	11

Table 4: Morphometric characteristics for the inferior limbal region.

Subject	Vessel Size(μm)		Vessel Depth(μm)		# of Vessels
	Mean Value ± SD	**Min – Max Values**	**Mean Value ± SD**	**Min – Max Values**	
1	24.847 ± 16.912	8.1 - 51.958	230.236 ± 145.218	74.934 - 518.479	8
2	16.087 ± 9.754	6.05 - 38.176	166.873 ± 105.098	47.315 - 416.746	10
3	24.958 ± 18.793	7.0625 - 70.12	188.463 ± 156.151	57.11 - 550.355	10
4	18.525 ± 14.415	5.2 - 54.6	199.496 ± 110.725	92.428 - 463.794	13
5	21.838 ±17.022	5.2 - 54.755	199.08 ± 107.900	117.382 - 483.293	13
6	35.409 ± 27.306	9.317 - 116.083	269.06 ± 135.610	49.867 - 531.087	15
7	18.618 ± 14.924	6.14 - 62.452	204.464 ± 166.426	56.054 - 526.446	18
8	19.476 ± 13.398	7.44 - 63.72	214.955 ± 122.802	56.992 - 567.941	17
9	28.165 ± 16.613	9.552 - 63.335	219.221 ± 187.027	57.231 - 590.657	12
10	29.064 ± 21.883	7.352 - 76.454	194.349 ± 88.465	82.436 - 440.261	15
11	22.81 ± 20.724	6.37 - 73	204.027 ± 126.135	64.215 - 504.712	13
12	18.824 ± 12.624	5.507 - 38.206	172.566 ± 90.8099	66.324 - 373.919	9
13	26.924 ± 17.356	6.14 - 55.237	182.181 ± 129.408	52.644 - 399.8	12
14	25.212 ± 20.724	8.455-63.667	210.953 ± 181.896	48.474 - 642.289	8

Vessel size measurements (Figure 11) within the superior limbus were repeatable between multiple measurements of the same vessel. The concordance correlation coefficient was 0.958 (95% CI, 0.935 to 0.964). One data point (shown with the arrow) appears to be an outlier and thus a trimmed concordance correlation coefficient was calculated to be 0.978 (95% CI, 0.959 to 0.988).

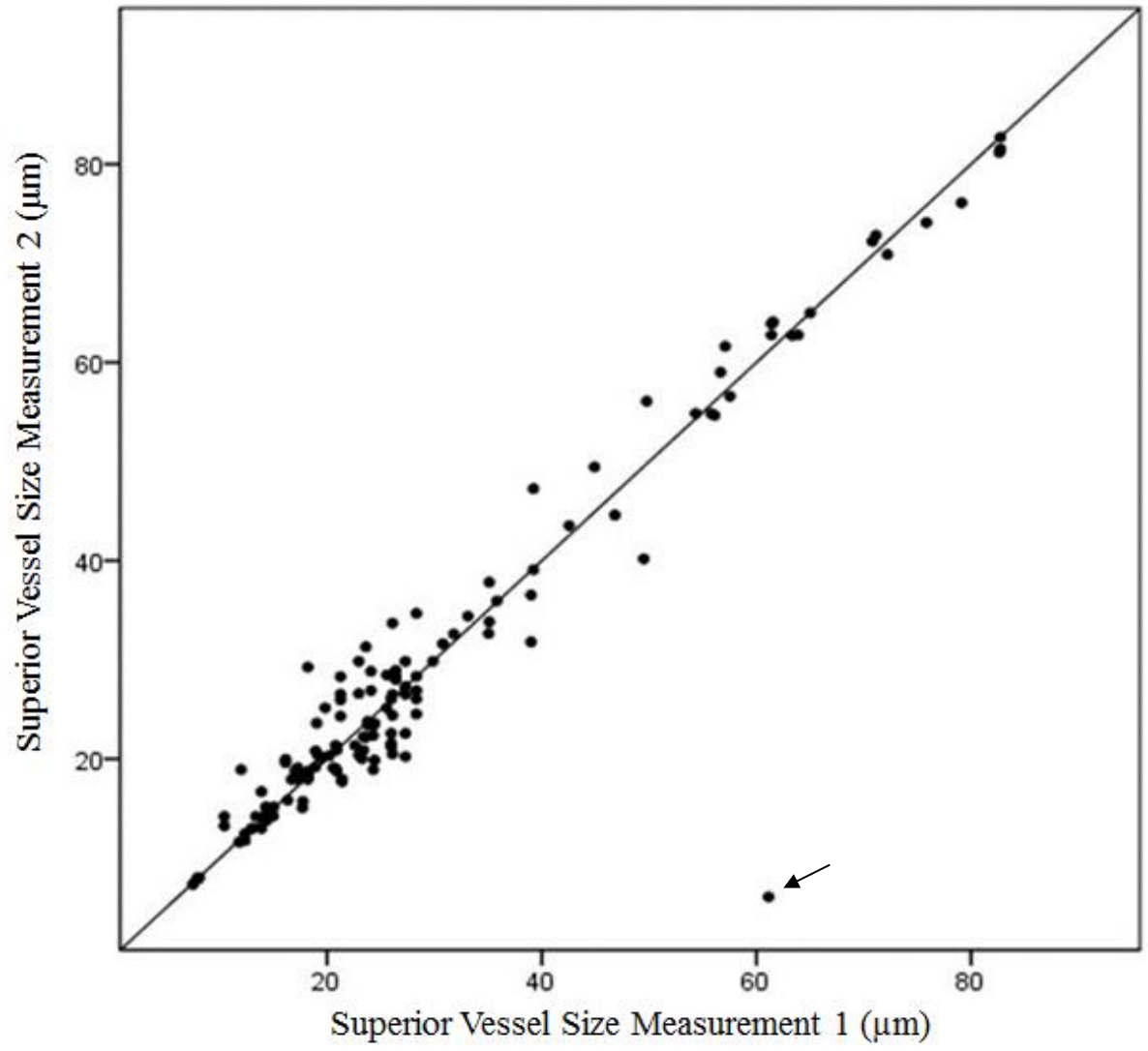

Figure 11: Repeatability of vessel size measurements in the superior limbus.

For the inferior limbus, vessel size measurements (Figure 12) were repeatable between multiple measurements of the same vessel. The concordance correlation coefficient was 0.994 (95% CI, 0.991 to 0.995).

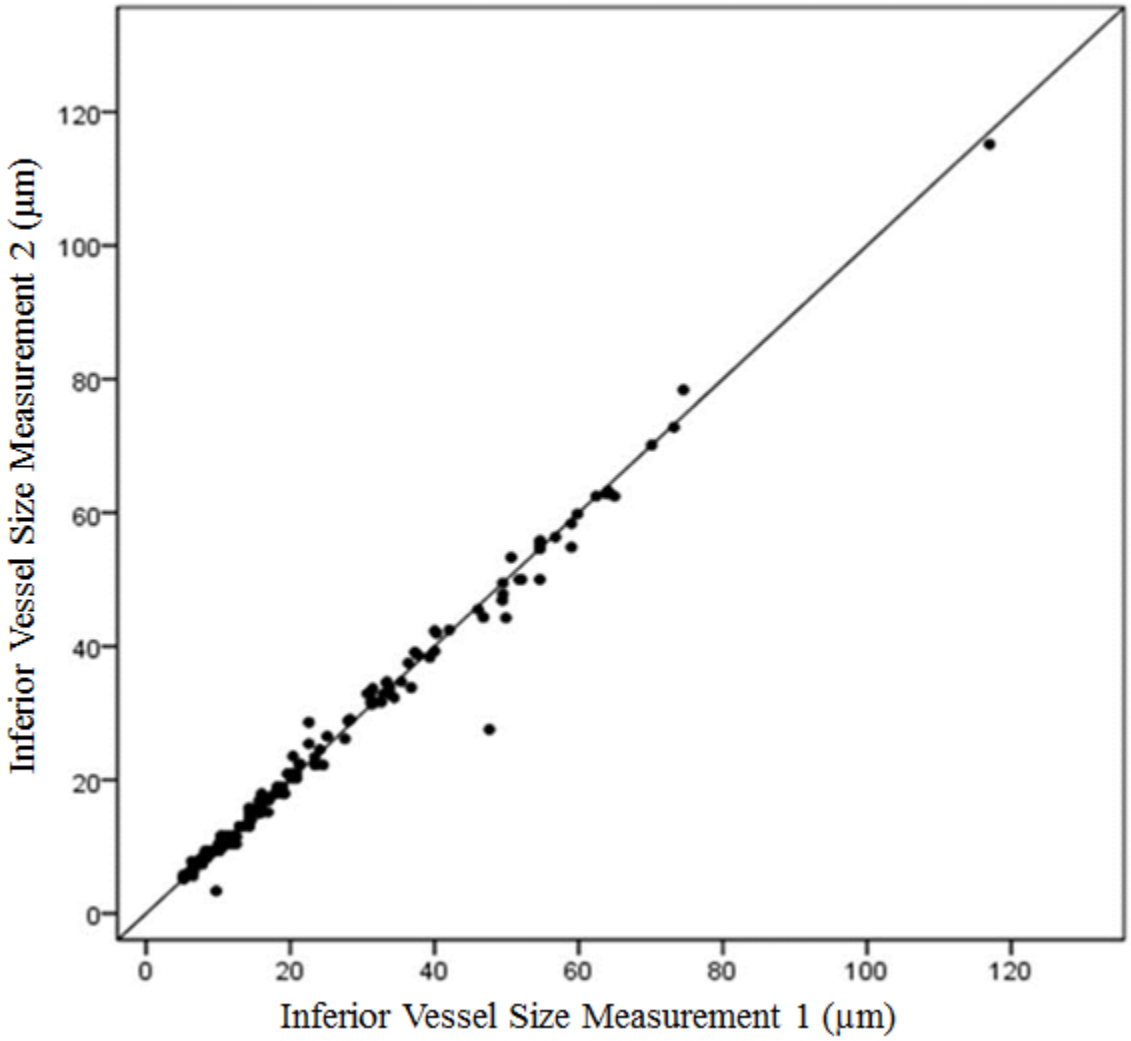

Figure 12: Repeatability of vessel size measurements in the inferior limbus.

Displayed in Figure 13 (below) is information about the vessel diameters found at both the superior and inferior limbus. The vessels within the superior limbus were larger than the vessels found in the inferior limbus (RM-ANOVA POS p = 0.004).

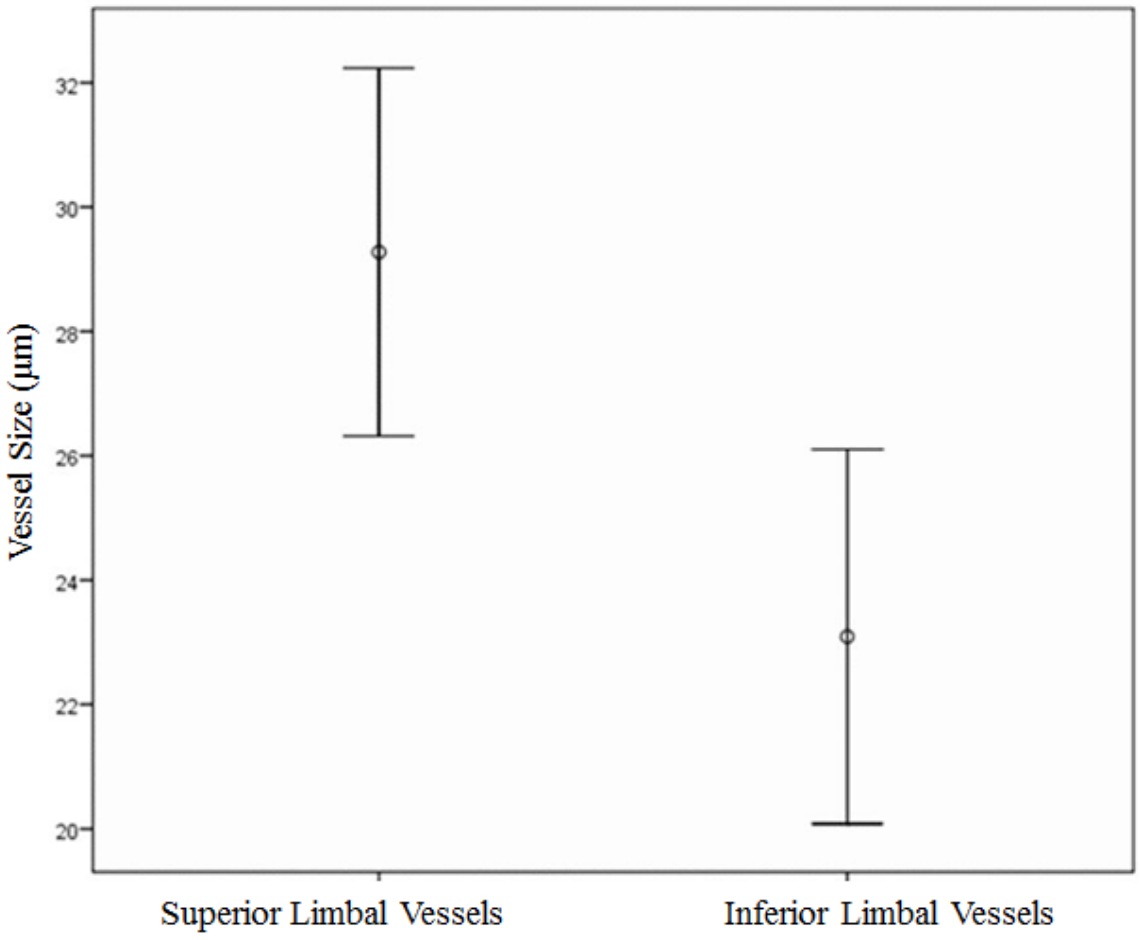

Figure 13: Superior and inferior limbal mean vessel sizes. The error bars show the 95% confidence interval of the mean.

For the superior limbus, vessel depth measurements (Figure 14) were repeatable between multiple measurements of the same vessel. The concordance correlation coefficient was 0.998 (95% CI, 0.997 to 0.999).

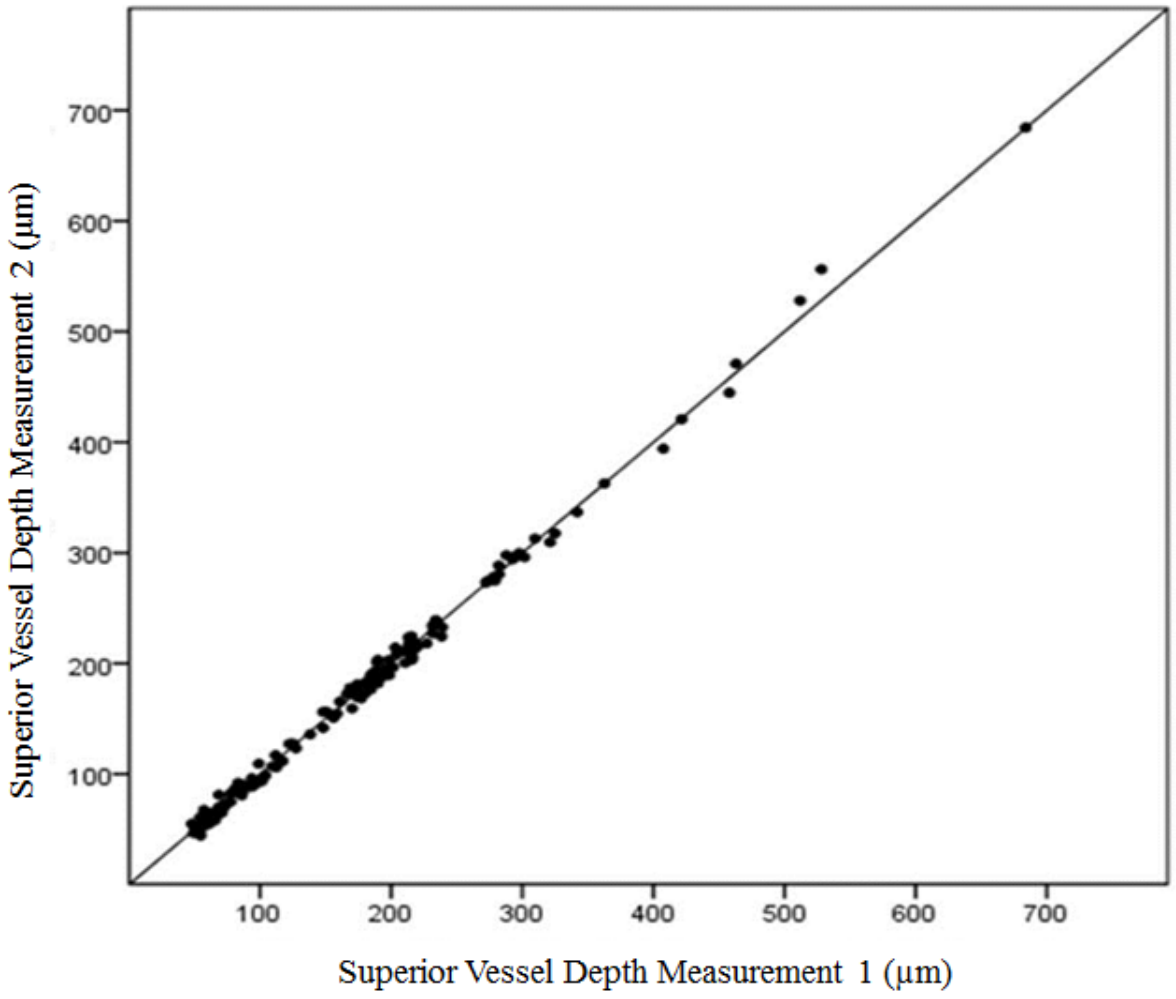

Figure 14: Repeatability of vessel depth from the anterior ocular surface in the superior limbus.

Measurements of vessel depth within the inferior limbus (Figure 15) were repeatable between multiple measurements of the same vessel. The concordance correlation coefficient was 0.998 (95% CI, 0.997 to 0.998).

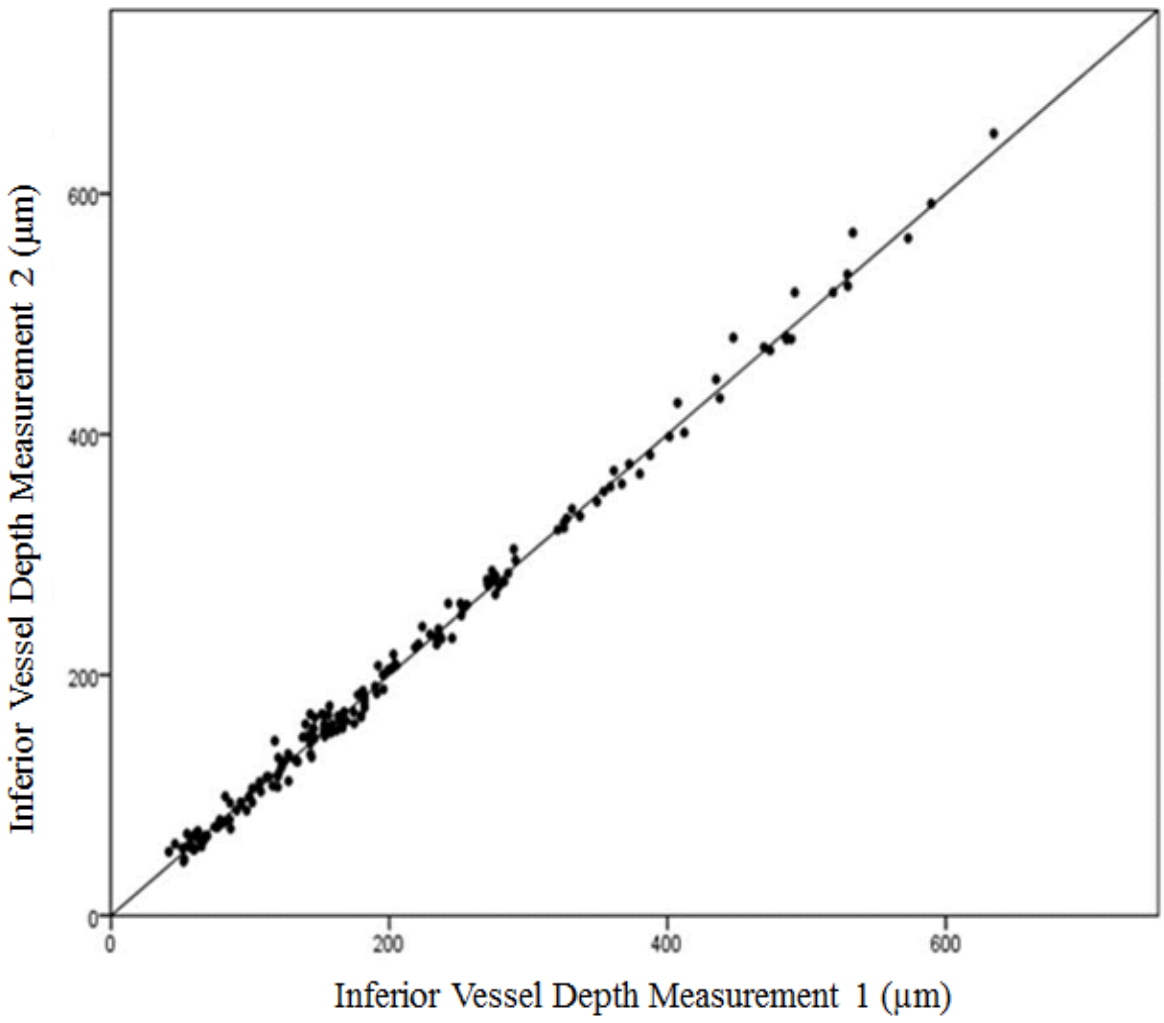

Figure 15: Repeatability of vessel depth from the anterior ocular surface in the inferior limbus.

Displayed in Figure 16 (below) is information about the vessel depth found at both the superior and inferior limbus. The vessels within the inferior limbus were on average deeper than the vessels found within the superior limbus (RM-ANOVA POS p = 0.041).

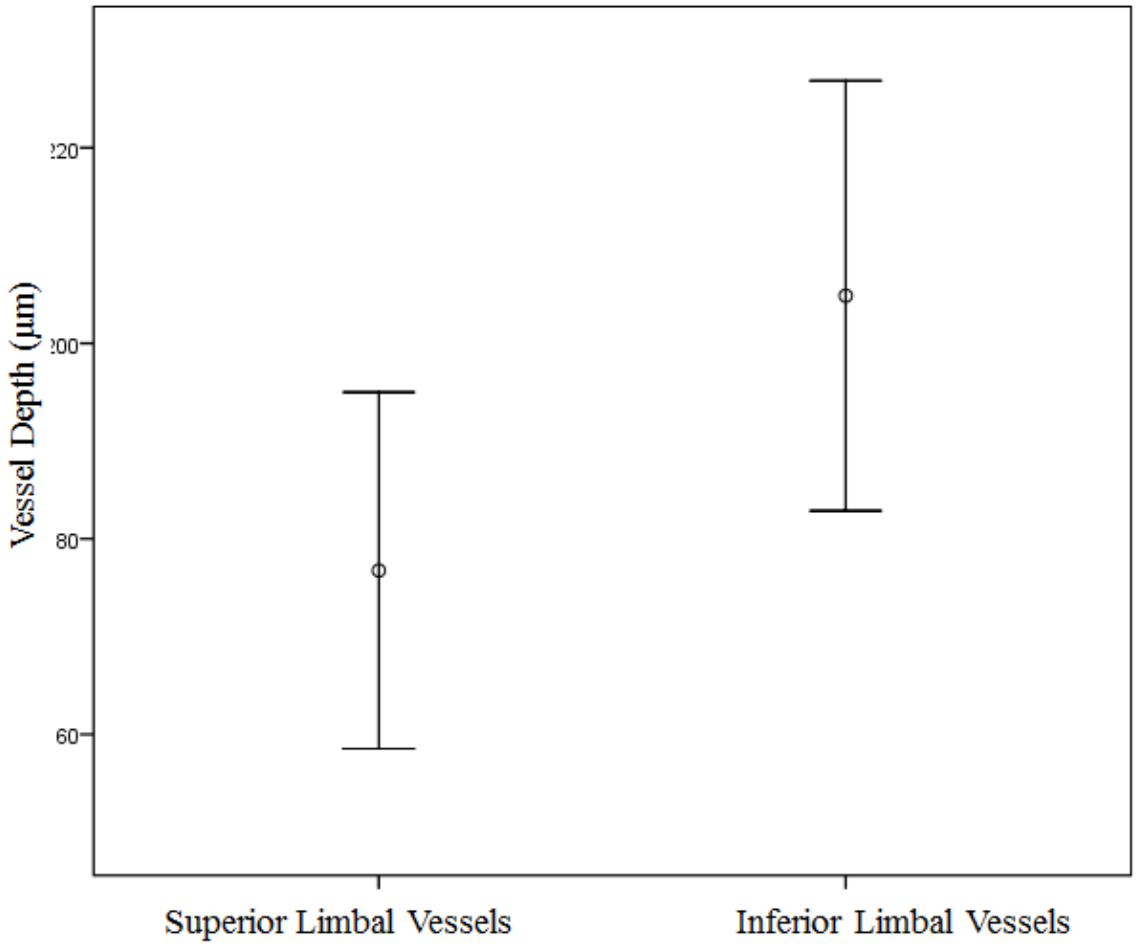

Figure 16: Superior and inferior limbal mean vessel depths. The error bars show the 95% confidence interval of the mean.

There was a positive linear relationship between limbal vessel depth and size within the superior limbus (Figure 17). The Pearson correlation coefficient for the superior limbus was 0.803.

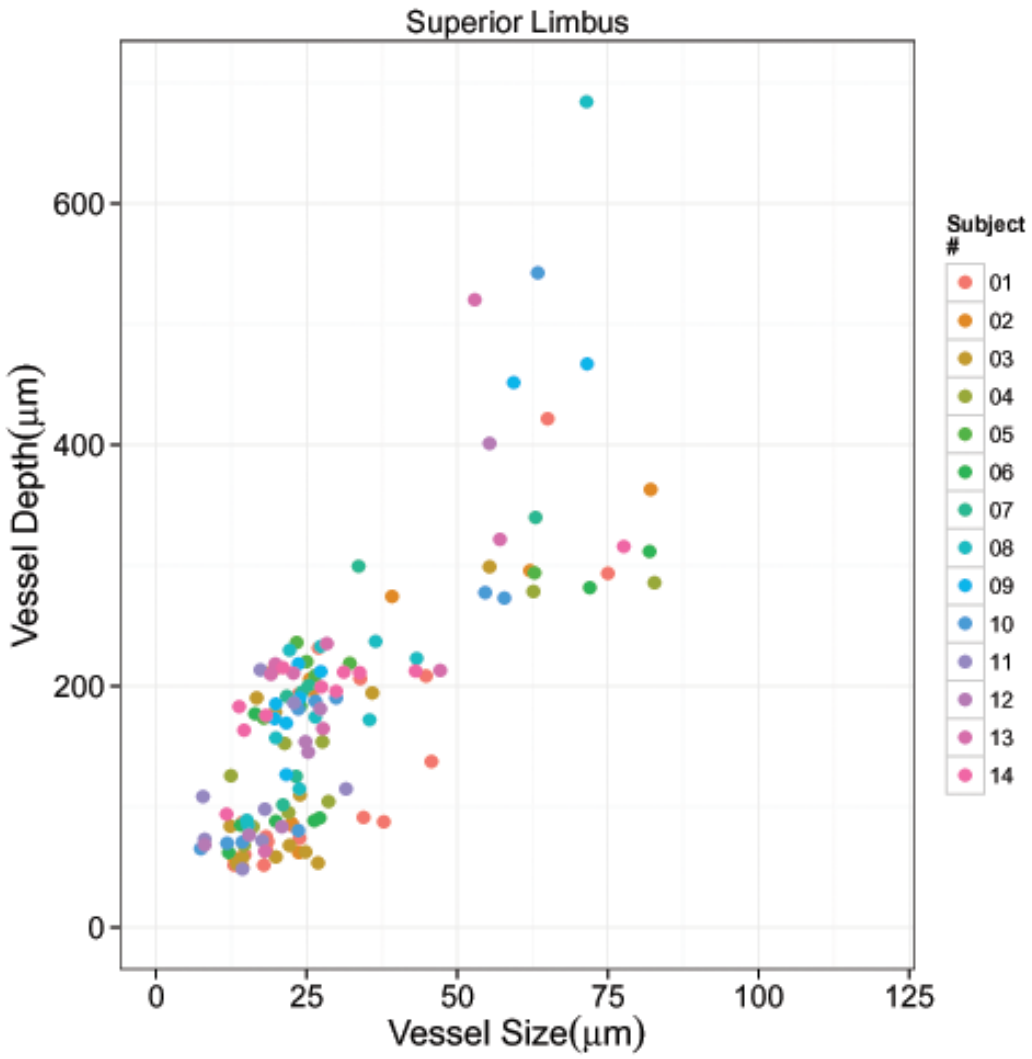

Figure 17: Scatterplot of the relationship between vessel depth and size of the superior limbus.

Table 3: Legend and subject-wise correlation coefficients for the linear relationship between vessel depth and size within the superior limbus.

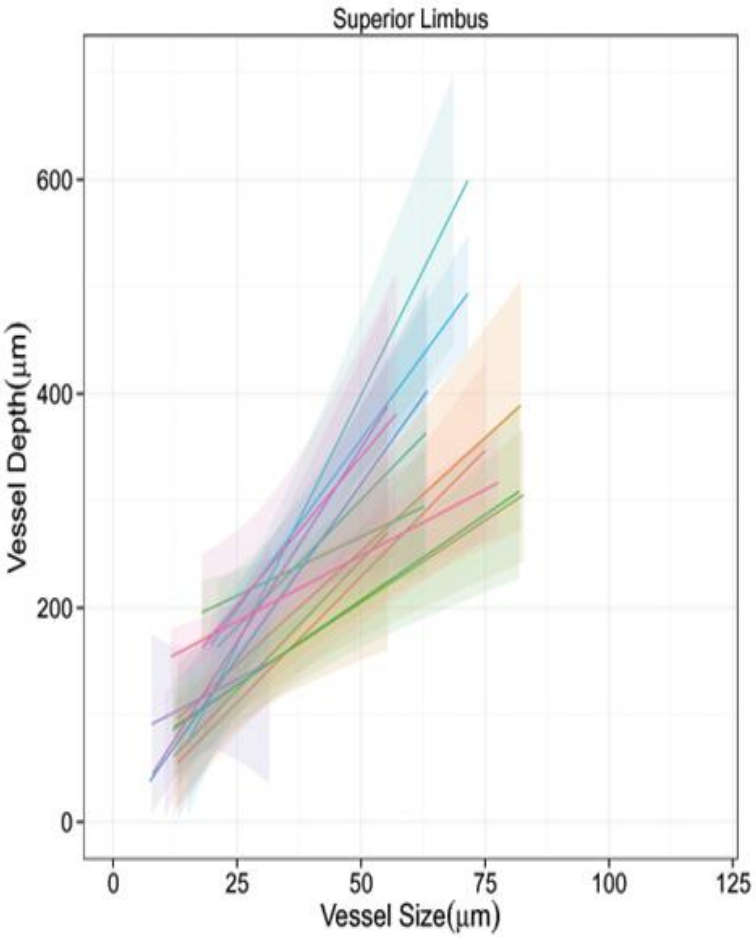

Subjects	Correlation coefficient
1	0.816
2	0.848
3	0.725
4	0.926
5	0.900
6	0.888
7	0.831
8	0.917
9	0.977
10	0.892
11	0.327
12	0.924
13	0.715
14	0.881

Table 3

Figure 18: Subject-wise correlation lines showing the relationship between vessel depth and size of the superior limbus per subject.

There was a positive linear relationship between limbal vessel depth and size within the inferior limbus (Figure 19). The Pearson correlation coefficient is 0.754.

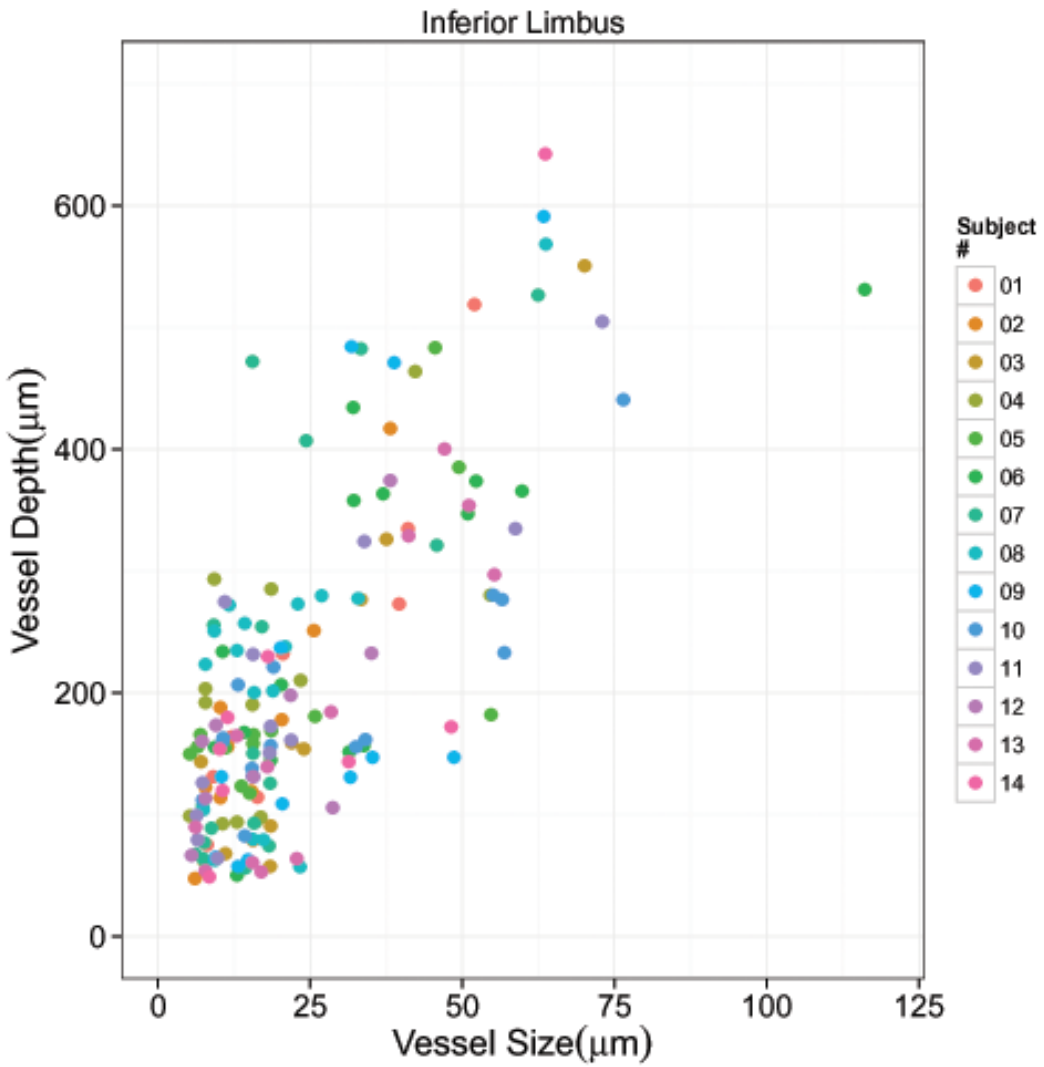

Figure 19: Scatterplot of the relationship between vessel depth and size of the inferior limbus.

Table 4: Legend and subject-wise correlation coefficients for the linear relationship between vessel depth and size within the inferior limbus.

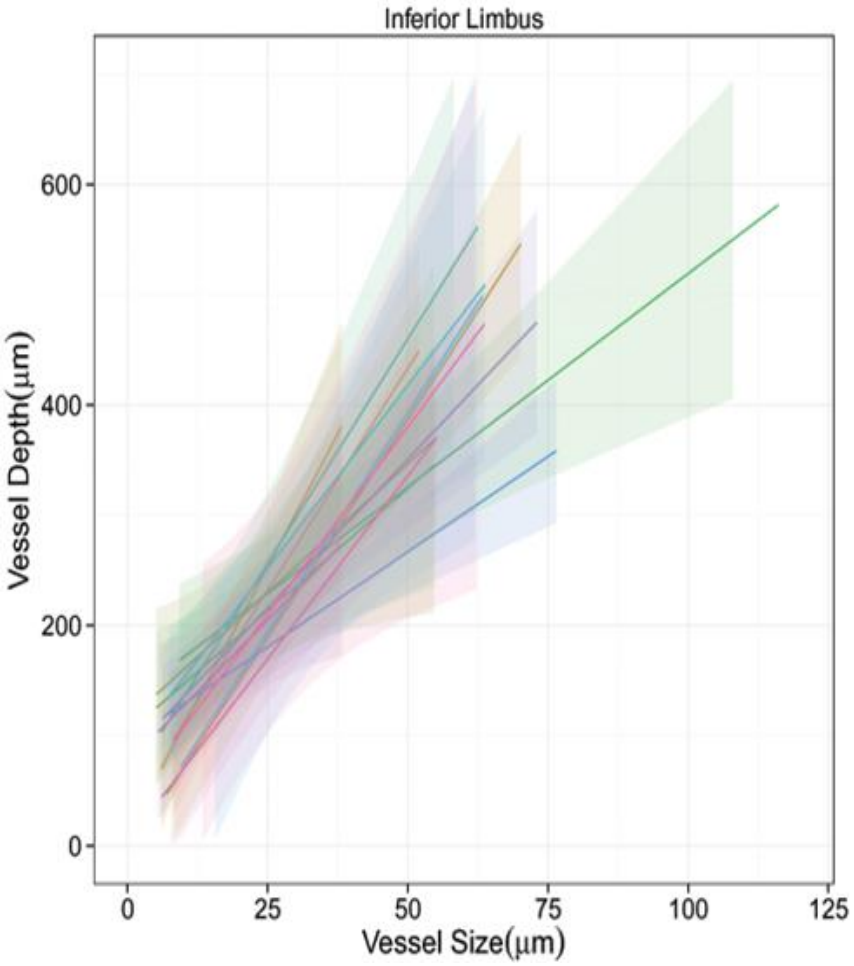

Subjects	Correlation coefficient
1	0.939
2	0.895
3	0.952
4	0.608
5	0.701
6	0.779
7	0.729
8	0.724
9	0.705
10	0.854
11	0.886
12	0.723
13	0.892
14	0.777

Table 4

Figure 20: Subject-wise correlation lines showing the relationship between vessel depth and size of the inferior limbus per subject.

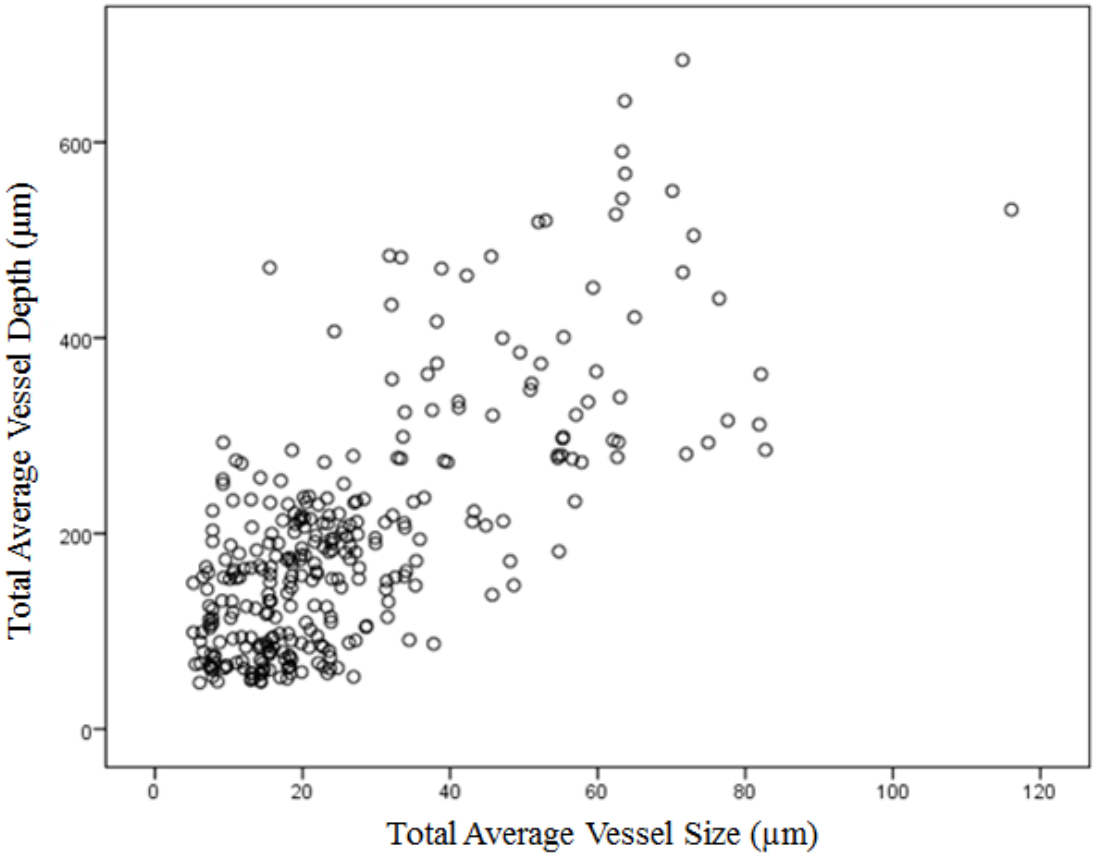

Figure 21: Scatterplot of the relationship between vessel depth and size of the superior and inferior limbus.

Chapter 5
Discussion

5.1 Repeatability of UHR-OCT measurements

To date there is little published work on the test and retest reliability of OCT measurements on vessel characteristics within the limbus. The results from this study indicate that measurements of vessel depth and diameter within the human limbus can be carried out in vivo using UHR-OCT and are repeatable.

With respect to vessel size as indicated for the superior and inferior limbus (Figures 11 and 12) respectively, it is clear that the initial and the second measurements of the same vessel diameter were very similar. It is also interesting to note that repeatability in the inferior limbus (ccc = 0.994) was higher than that of the superior limbus. This can be due to a few factors, with the most probable reason being the existence of a clear outlier (Figure 11) in the vessel diameter measurements of the superior limbus. This vessel size, though quite large when compared to the other vessels is suspected to be an aqueous vein due to its size and location within the deeper segments of the limbus where the UHR-OCT gradually losses signal due to the scattering of light. It is worthy to note that after a trimmed analysis of the ccc was performed on the same data a higher ccc value of 0.978 was the result, yet this value remains lower than that of the inferior limbus. This raises the issue that the reduction in repeatability value for the superior limbus may have some other underlying reason.

During the image acquisition process, imaging the inferior limbus tends to be much easier than imaging of the superior limbus because one has to invert the upper eyelid to gain easy access to the whole superior limbus, this can sometimes be uncomfortable as a greater ocular

surface area is exposed to the atmosphere resulting in dry eye sensation, tearing and other unwanted sensations (Stern et al., 1998). Compression effects may also be experienced through the eversion of the upper eyelid and this may be consistent over multiple measures thereby influencing superior vessel measurement results. It is also worthy to note that studies have shown the superior limbal area to be relatively thicker than the inferior limbal area (Erickson, Comstock, & Zantos, 2002; Remon et al., 1992). On the other hand, in most instances when imaging the inferior limbus the subject only looks upwards and the whole inferior limbus is exposed, in other cases a slight depression of the lower eyelid is made to ensure optimal imaging. The difficulty in imaging the superior limbus coupled with its greater thickness and lid eversion associated compression effects, may have an impact on the end images which may perhaps influence the repeatability of measurements made in the superior limbus.

From Figures 14 and15, the repeatability measurements for both superior and inferior vessel depth measurements respectively, were high. Also, Figures 18 and 20, seem to show a positive linear relationship between vessel depth and size, within all subjects of the study, for both the superior and the inferior limbus. With the exception of one subject whose positive linear relationship between vessel depth and size was low ($r < 0.5$) in the superior limbus alone, all other within subject correlation values of vessel depth and size were high across both the superior and inferior limbus ($r > 0.5$).

Limbal vessel depth measurements are important as it provides some inference as to the function of a vessel (E. B. Papas, 2003), thus, a means to consistently measure this characteristic is beneficial. A review of Figures 17-20 gives insight to the possibility of being

able to use vessel depth to determine corresponding vessel size because of the high positive linear relationship between size and depth across subjects for both the superior and inferior limbus. This is of marked importance as one might be able to estimate the vessel size of deeper vessels that are not within the scanning depth range of the UHR-OCT. Additionally, information about vessel size is related to aqueous drainage (Johnson & Kamm, 1983; Wang, Chintala, Fini, & Schuman, 2001) which further has implications on some ocular pathology such as glaucoma (Gould, Smith, & John, 2004). Limbal vessel depth and size give information about the anatomic and physiological properties within the limbus (Van Buskirk, 1989; van der Merwe & Kidson, 2010) and this may be beneficial in the design and construction of glaucoma drainage implants and devices that aim to mimic the natural drainage process existent in the limbus (Hong, Arosemena, Zurakowski, & Ayyala, 2005; Molteno, 1969; Ritch & Klein, 1990).

The possible estimation of vessel size using vessel depth because of the discovered positive linear relationship between the two characteristics might prove to be a useful tool; from the author's experience it is less of a challenge to identify the depth of a vessel in a 2D OCT tomogram due to the distinct change in reflectivity clearly demarcating the walls of the vessels as observed in Figure 22. However, estimating vessel size in a 2D tomogram can sometimes prove challenging due to vessel tortuosity which causes rather elongated ellipses to represent vessels instead of the fairly circular boundaries that are associated with the lumen of vessels (van der Merwe & Kidson, 2010), (Figure 22, label C and D). A possible solution to this problem involves a complete 3D reconstruction of the OCT tomograms (Figure 23) followed by an oblique slice made through the area of the specific tomogram that

isolates the vessel of interest (Figure 24 and 25). At this point, a proper measurement of the vessel size can then be made. The ability to use vessel depth information to estimate vessel size can improve the speed of manual grading in future experiments involving UHR-OCT imaging of the limbal vessels as the 3D reconstruction with subsequent slicing and measurement can be eliminated.

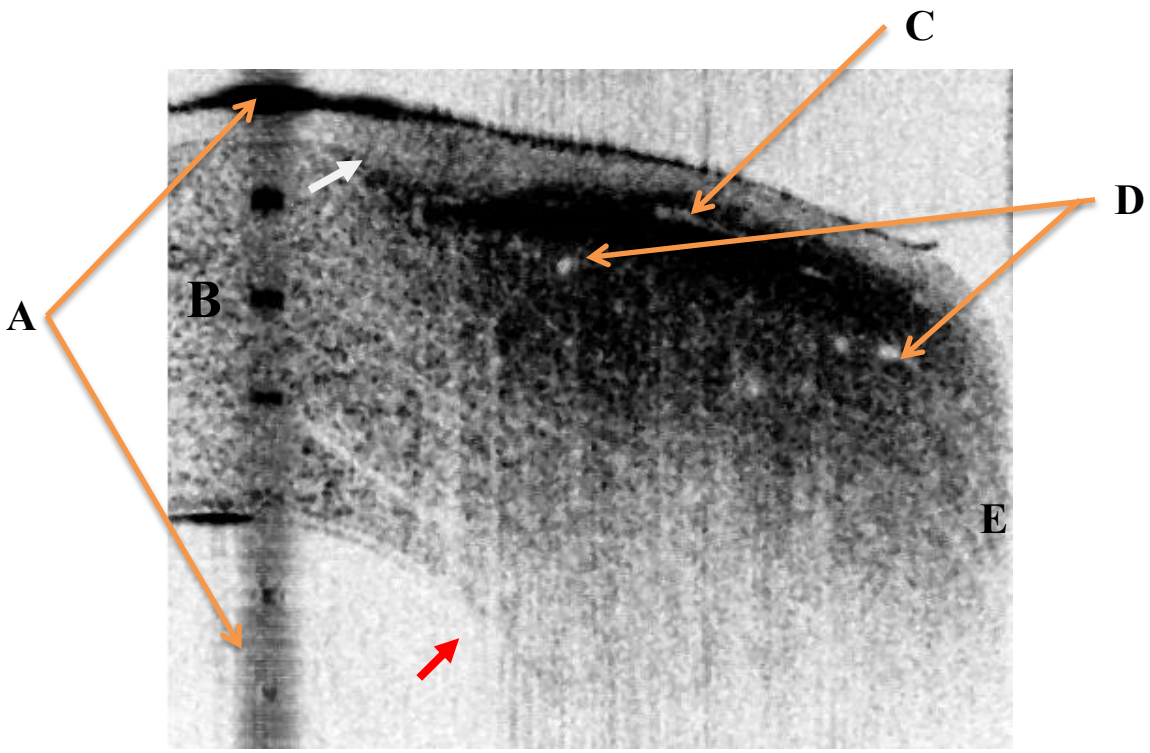

Figure 22: A UHR-OCT of the human limbus. **A** - specular reflection which indicates that the imaging was done approximately orthogonal to the limbus. **B** – peripheral cornea. The white and red arrows show the termination of the Bowman's membrane and Descemet's - endothelial complex respectively, both are landmarks for the corneo-limbal junction. **C** - limbal vessel, the size of this vessel cannot be properly estimated due to the shape so a

further 3D reconstruction is required to better judge the vessel diameter. **D** – limbal vessels whose diameter can be estimated with a circle or ellipse tool. **E** – sclera.

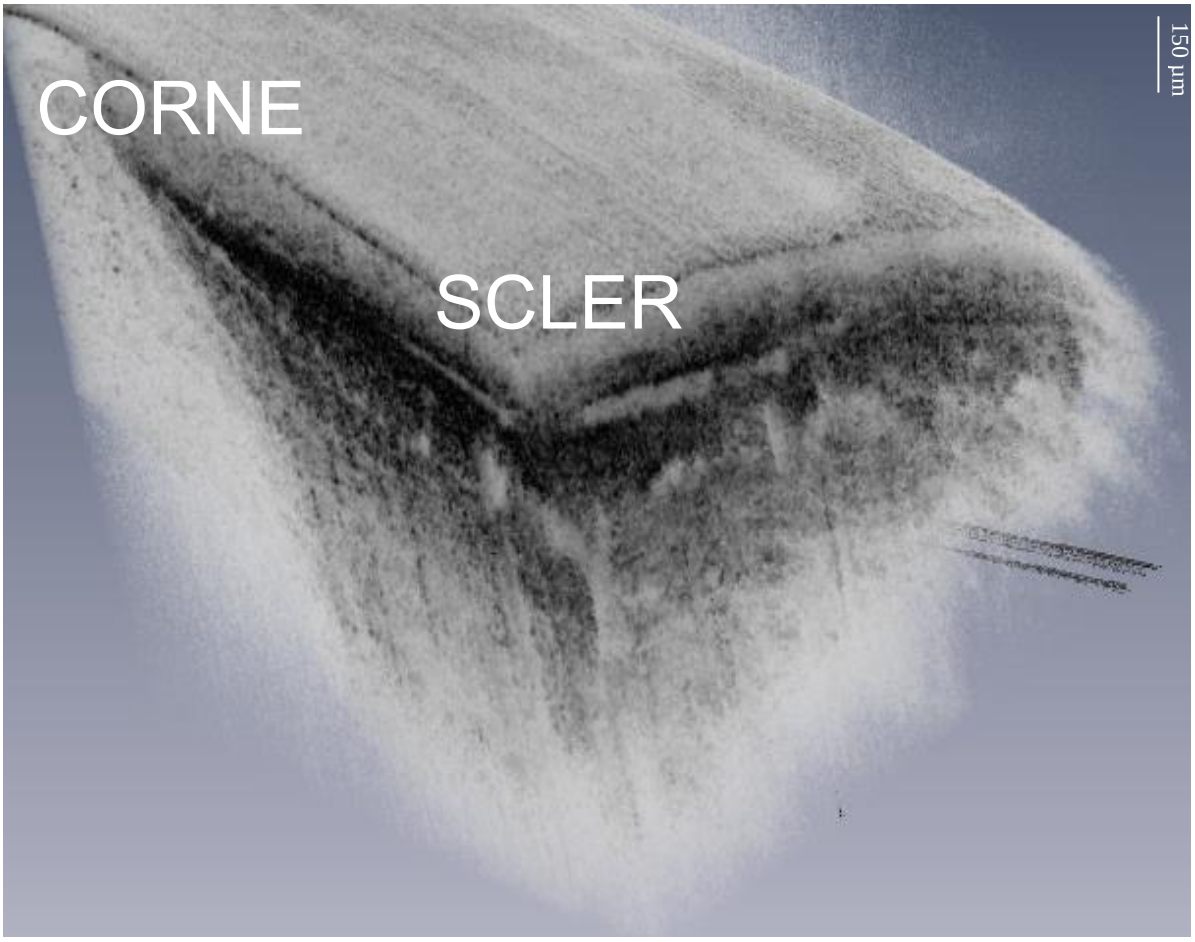

Figure 23: Three dimensional reconstruction of a set of UHR-OCT tomograms of which the tomogram from Figure 22 forms a part of. This reconstruction can be sliced at different angles and the vessels assessed and measured with the requisite ellipse or circle tool.

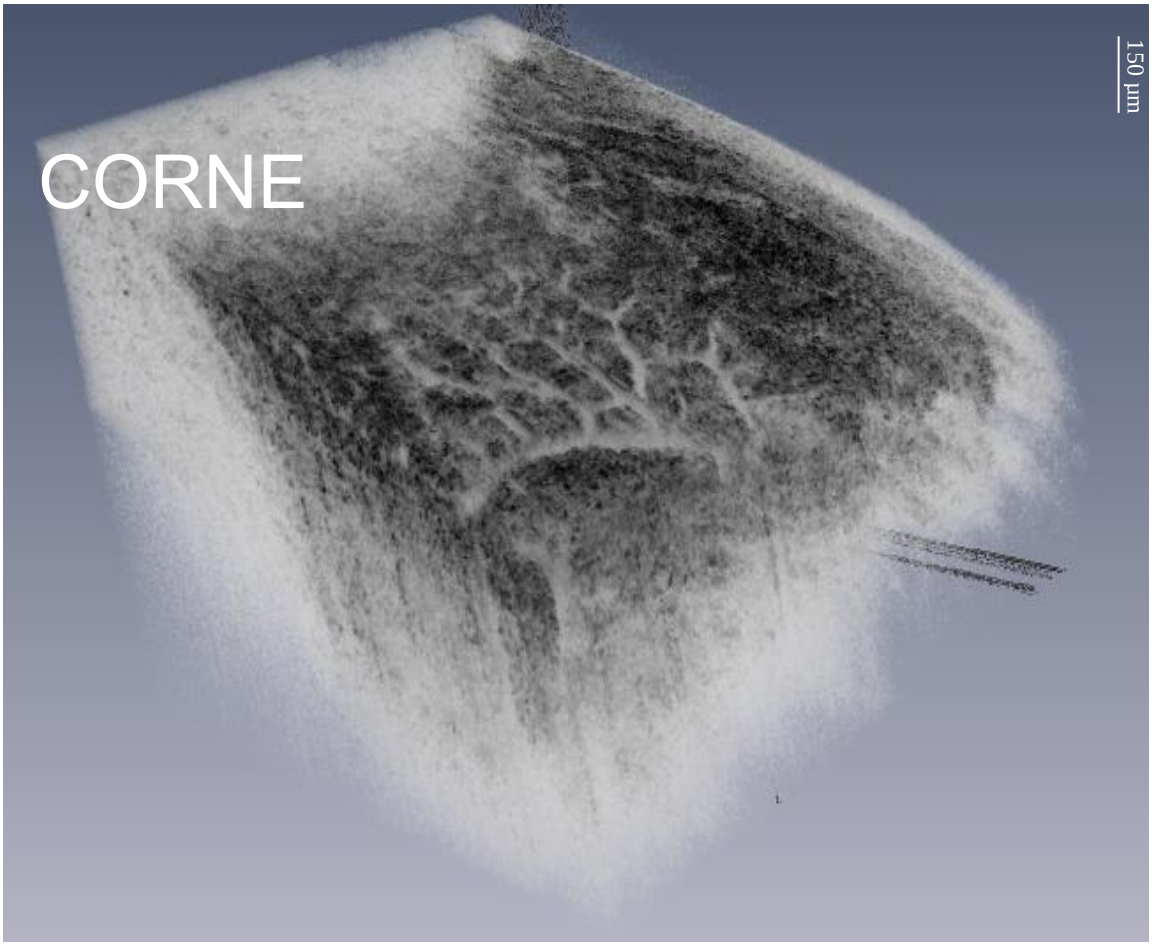

Figure 24: Three dimensional reconstruction of the limbus with the epithelium stripped through an oblique slice to reveal the vessel structure within the limbus.

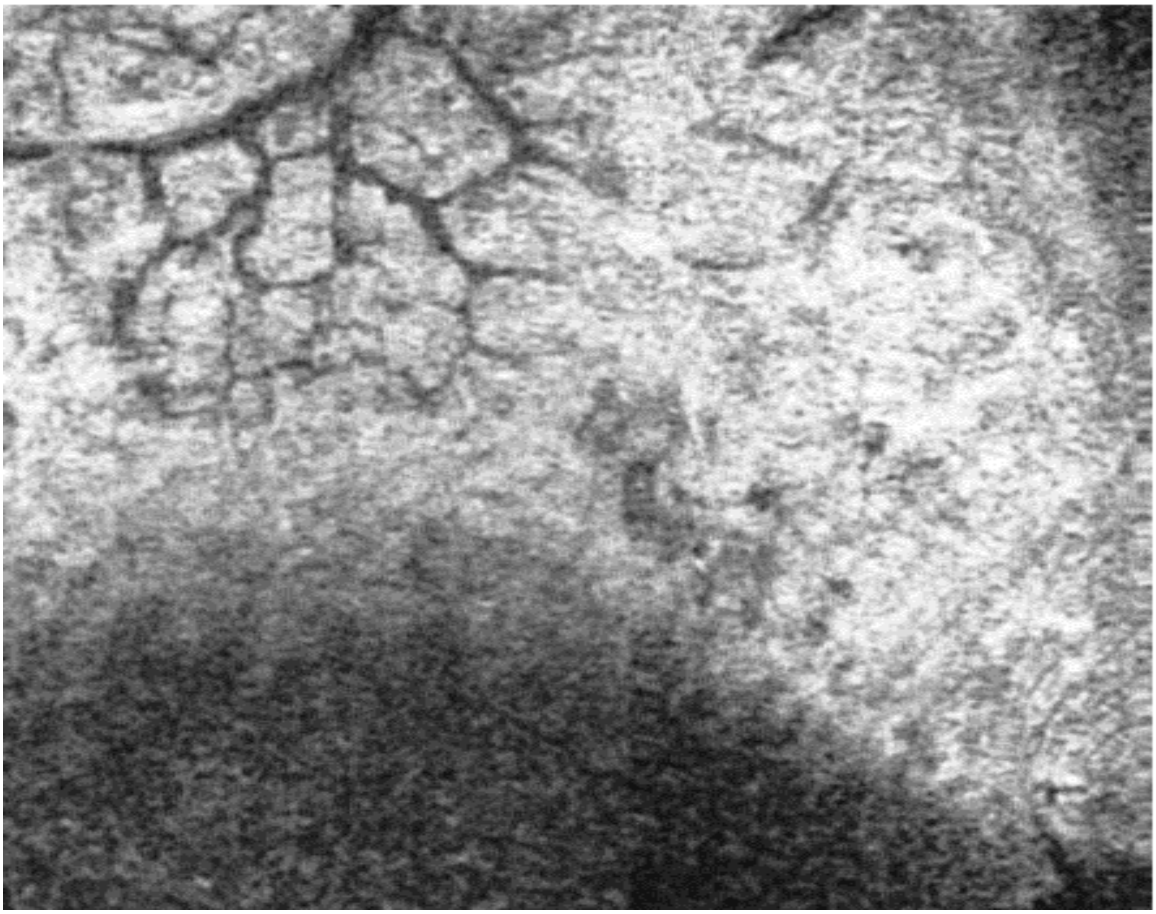

Figure 25: A section from the three dimensional reconstruction of the limbus in Figure 24 revealing the vessel structure within the limbus from an enface view.

Though the test and retest reliability of the repeated measurements of vessel size and depth within both the superior and inferior limbus proved to be very high, the ability for different observers to provide consistent estimates of vessel size / depth of the same vessel was not assessed. Future experimentation to assess this characteristic will help eliminate current study limitations such as observer bias induced by having only one rater (Stemler, 2004).

From the results presented in this study (Figures 11,12,14 and 15), measurements of limbal vessel depth and size are deemed repeatable and as such all further calculations presented in this study were computed based on the average values of measurements one and two of vessel size and likewise for vessel depth.

5.2 Morphologic characteristics of the limbus

Morphometry involves the precise study of anatomical character by measurement (Rohlf & Bookstein, 1990). Though information about the form and structure of vessels observed in-vivo using ultra-high resolution optical coherence tomography can be found in recent literature (Bizheva et al., 2011; Grulkowski et al., 2009; Grulkowski et al., 2011; Li et al., 2011), the quantitative analysis of the size and depth of vessels within the limbus are yet to be addressed. To the author's knowledge, this is the first study that provides quantitative details and differences about the size and depth of vessels that are located within the superior and inferior human limbus using ultra-high resolution optical coherence tomography. The findings of this study suggest that the vessels found in the superior limbus are on average greater in size and closer to the ocular surface than the vessels located within the inferior limbus.

The least number of vessels per subject was counted in the superior limbus and the greatest amount of vessels per subject was counted in the inferior limbus. For the superior limbus, there were on average, about 9 vessels per subject while for the inferior limbus there were on average, approximately 13 vessels per subject (Tables 1 and 2). It has been previously reported that the limbal region contains at least 4 episcleral veins (Oyster, 1999), but the approximate number of arterioles have not been stated. Though the average quantity of vessels per subject appear to be greater in the inferior limbus, than the superior limbus, the size of the vessels within the superior limbus being significantly larger (Figure 13) might contribute to an adaptive mechanism described below.

From Figure 13 it can be deduced that there is a difference in vessel size in relation to the position they are located in as, on average, the superior limbus possess larger vessels than the inferior limbus. There is a greater demand for oxygen in the region around the superior limbus as compared to other parts of the limbus (W. Benjamin & Hill, 1988; W. Benjamin & Rasmussen, 1988; W. J. Benjamin & Ruben, 1995; Fitzgerald & Efron, 1986) and this may account for the difference in vessel sizes existent in the two limbal regions. Another contributing factor to vessel size difference between the superior and inferior limbus may be attributed to the role of the upper eyelid as it constantly covers the superior limbal region and prevents its exposure to atmospheric oxygen (Baum, 1997). The difference in vessel size between the superior and inferior limbus may thus be an adaptation to the chronic hypoxia caused by the upper eyelid's constant coverage of the superior limbus.

A previous study by Simpson et al, 2012 (Simpson et al., 2012) supported the possible difference in limbal structure under the upper eyelid and proposed further investigation into

limbal structure under the upper eyelids. Similarly, in accordance with the results of this study, it has previously been suggested that one of the main differences between superior and inferior limbal morphometry involved episcleral and conjunctival vessel size, with superior episcleral and conjunctival vessels being significantly larger than their corresponding inferior vessels (Alabi, Hutchings, Bizheva, Feng, & Simpson, 2013).

Figure 16 represents an analysis of vessel depth measurements relative to the ocular surface of the superior and inferior limbus. It appears that vessels in the inferior limbus are on average found deeper within the limbus, and away from the ocular surface than superior limbal vessels. Since both superior and inferior limbal vessel depth measurements appears to be related to their corresponding limbal vessel size measurements, it can be assumed that the earlier discussed factors of oxygen intake (W. Benjamin & Hill, 1988; W. Benjamin & Rasmussen, 1988; W. J. Benjamin & Ruben, 1995; Fitzgerald & Efron, 1986) and eyelid coverage (Baum, 1997) play a role in superior limbal vessels being closer to the ocular surface. Parameters of vessel depth and size acquired from this study may also influence future interventions for vascular disorders involving the anterior segment (Kehlet Barton, Izatt, Kulkarni, Yazdanfar, & Welch, 1999).

5.3 Limitations and future studies

A drawback to this study was the inability to measure vessel size and depth within the nasal and temporal limbus. While some studies have briefly looked at temporal and nasal limbal vasculature (Bizheva et al., 2011), there is the need to quantitatively assess the size and depth of vessels across all four quadrants of the eye.

Furthermore, this study was unable to differentiate arteries from veins, and veins carrying blood from aqueous veins. This task is quite challenging as most of the veins found in the limbal region carry both blood and aqueous fluid with exception of the veins emanating directly from the canal of Schlemm that solely carry aqueous fluid (Oyster, 1999). Information about the size and location of a vessel may play a fundamental role in categorizing vessels as either blood or aqueous veins (Gong, Tripathi, & Tripathi, 1996), thus, further investigation is required for the possible identification of vessels as blood or aqueous veins based on these characteristics. The direction of blood flow within arteries and veins may also aid in the categorization of vessels within the limbus (Oyster, 1999).

Finally, Figure 21 shows a scatterplot of all the vessel size and depth measurements. From the plot one might be able to locate two major demarcations, possibly based on depth and size. In the scatterplot vessels that have a depth less than roughly 300 μm and a size less than 40 μm seem to appear clumped into one cluster, while on the other hand, most of the vessels over approximately 300 μm in depth and 40 μm in size seem to aggregate into another cluster. This could be a possible indication as to the thickness of the conjunctiva which would contain the conjunctival vessels and the deeper layers of the limbus housing larger vessels (van der Merwe & Kidson, 2010; Zhang et al., 2011).

This study did not differentiate between possible conjunctival vessels, which would appear more towards the ocular surface and the deeper episcleral vessels (Oyster, 1999). Future studies of this nature should incorporate a means of dividing vessels based how deep they are within the limbus.

Chapter 6
Conclusions

The goal of this study was to characterize and compare the vessels of the superior and inferior limbus using UHR-OCT. From the results obtained from this study, the UHR-OCT was capable of imaging and measuring morphometric characteristics such as size and depth of vessels within the limbus in a repeatable manner. Further results acquired from this study suggest a positive linear relationship between vessel depth and size, both within and between subjects. Additionally, a difference in the size and depth of vessels across different positions of the limbus was identified. While the vessels within the superior limbus were on average larger than the vessels found in the inferior limbus, the vessels within the inferior limbus were on average deeper than the vessels found within the superior limbus. These differences might suggest a greater demand for oxygen in the region around the superior limbus as compared to other parts of the limbus. The differences in vessel size and depth might also be indicative of an adaptive mechanism to the chronic hypoxia caused by the upper eyelid's constant coverage of the superior limbus. This study was unable to extend the measurements of vessel size and depth to the nasal and temporal limbus and as such there is the need to quantitatively assess and investigate the size and depth of vessels across all four quadrants of the eye in future studies. Furthermore, this study did not group vessels based on size and depth information acquired, and further investigation is required into the categorization of vessels within the limbus using UHR-OCT.

Appendix

SINAUER ASSOCIATES, Inc. • Publishers • P.O. Box 407 • Sunderland, MA 01375-0407

Telephone: (413) 549-4300
Fax: (413) 549-1118
E-mail: orders@sinauer.com

PERMISSIONS AGREEMENT

August 29, 2013

Permission granted to:
Emmanuel Alabi
200 University Avenue West
Waterloo, ON N2L 3G1
CANADA

Email: ebalabi@uwaterloo.ca

Material to be reproduced:
Oyster: *The Human Eye: Structure and Function*
Figure 6.14, page 263

To be reproduced in the work:
Emmanuel Alabi's MSc Thesis entitled "Characterization of the Limbal Vasculature using UHR-OCT" to be published by the University of Waterloo (print and electronic)

Sinauer Associates owns copyright to the material described above and hereby grants permission for the one-time use of the material as specified, and for nonexclusive world rights provided that full and appropriate credit is given to the original source and that the work is for NON-COMMERCIAL use only. Please request permission for further use in subsequent editions, translations, or revisions of the work.

References

Aharinejad, S., MacDonald, I. C., Schmidt, E. E., Bock, P., Hagen, D., & Groom, A. C. (1993). Scanning and transmission electron microscopy and high resolution intravital video-microscopy of capillaries in the mouse exocrine pancreas, with special emphasis on endothelial cells. *The Anatomical Record, 237*(2), 163-177.

Alabi, E., Hutchings, N., Bizheva, K., Feng, Y., & Simpson, T. (2013). Superior and inferior limbal epithelial and vascular structure characterized using ultra-high resolution optical coherence tomography [Abstract]. *ARVO Poster, 2590* (D0390).

Al-Aqaba, M. A., Fares, U., Suleman, H., Lowe, J., & Dua, H. S. (2010). Architecture and distribution of human corneal nerves. *British Journal of Ophthalmology*, *94*(6), 784-789.

Allemann, N., Chamon, W., Silverman, R. H., Azar, D. T., Reinstein, D. Z., Stark, W. J., & Coleman, D. J. (1993). High-frequency ultrasound quantitative analyses of corneal scarring following excimer laser keratectomy. *Archives of Ophthalmology*, *111*(7), 968.

Amann, J., Holley, G. P., Lee, S. B., & Edelhauser, H. F. (2003). Increased endothelial cell density in the paracentral and peripheral regions of the human cornea. *American Journal of Ophthalmology, 135*(5), 584-590.

Ascher, K. (1953). Aqueous veins: Their status eleven years after their detection. *Archives of Ophthalmology, 49*(4), 438.

Ashton, N. (1951a). Anatomical study of Schlemm's canal and aqueous veins by means of neoprene casts: Part I. aqueous veins. *The British Journal of Ophthalmology, 35*(5), 291.

Ashton, N. (1951b). Anatomical study of Schlemm's canal and aqueous veins by means of neoprene casts: Part I. aqueous veins. *The British Journal of Ophthalmology, 35*(5), 291.

Baum, J. L. (1997). Prolonged eyelid closure is a risk to the cornea. *Cornea, 16*(6), 602-611.

Benjamin, W., & Hill, R. (1988). Human cornea: superior and central oxygen demands. *Graefe's Archive for Clinical and Experimental Ophthalmology*, *226*(1), 41-44.

Benjamin, W., & Rasmussen, M. (1988). Oxygen consumption of the superior cornea following eyelid closure. *ActaOphthalmologica, 66*(3), 309-312.

Benjamin, W. J., & Ruben, C. M. (1995). Human corneal oxygen demands at superior, central, and inferior sites. *Journal of the American Optometric Association*, *66*(7), 423-428.

Bizheva, K., Hutchings, N., Sorbara, L., Moayed, A. A., & Simpson, T. (2011). In vivo volumetric imaging of the human corneo-scleral limbus with spectral domain OCT. *Biomedical Optics Express, 2*(7), 1794-1802.

Bizheva, K., Lee, P., Sorbara, L., Hutchings, N., & Simpson, T. (2010). In vivo volumetric imaging of the human upper eyelid with ultrahigh-resolution optical coherence tomography. *Journal of biomedical optics*, *15*(4), 040508-040508.

Bloch, E. H. (1956). Microscopic observations of the circulating blood in the bulbar conjunctiva in man in health and disease. *Ergebnisse Der Anatomie Und Entwicklungsgeschichte, 35*, 1-98.

Boote, C., Dennis, S., Newton, R. H., Puri, H., & Meek, K. M. (2003). Collagen fibrils appear more closely packed in the prepupillary cornea: Optical and biomechanical implications. *Investigative Ophthalmology & Visual Science, 44*(7), 2941-2948.

Bron, A. J. (1997). In Tripathi B. J. (Ed.), *Wolff's anatomy of the eye and orbit*. London: London : Chapman & Hall Medical.

Burger, P. C., Chandler, D. B., Fryczkowski, A. W., & Klintworth, G. K. (1987). Scanning electron microscopy of micro corrosion casts: Applications in ophthalmologic research. *Scanning Microscopy, 1*(1), 223-231.

Choma, M. A., Hsu, K., & Izatt, J. A. (2005). Swept source optical coherence tomography using an all-fiber 1300-nm ring laser source. *Journal of Biomedical Optics, 10*(4), 44009-44010.

Choma, M., Sarunic, M., Yang, C., & Izatt, J. (2003). Sensitivity advantage of swept source and fourier domain optical coherence tomography. *Optics Express, 11*(18), 2183-2189.

Clivaz, X., Marquis-Weible, F., Salathe, R. P., & Gilgen, H. (1992). High- resolution reflectometry in biological tissues. *Optics Letters, 17*(1), 4.

Cox, G., & Sheppard, C. J. (2004). Practical limits of resolution in confocal and non-linear microscopy. *Microscopy Research and Technique, 63*(1), 18-22.

de Boer, J., Cense, B., Park, B., Pierce, M., Tearney, G., & Bouma, B. (2003). Improved signal-to-noise ratio in spectral-domain compared with time- domain optical coherence tomography. *Optics Letters, 28*(21), 2067-2069.

Dvorak-Theobald, G. (1934). Schlemm's canal: Its anastomoses and anatomic relations. *Transactions of the American Ophthalmological Society, 32*, 574.

Erickson, P., Comstock, T. L., & Zantos, S. G. (2002). Is the superior cornea continuously swollen? *Clinical & Experimental Optometry : Journal of the Australian Optometrical Association, 85*(3), 168-171.

Farjo, A., McDermott, M., & Soong, H. (2009). Corneal anatomy, physiology, and wound healing. *Ophthalmology 44(2),* 203-208.

Fawcett, D. W. (1963). Comparative observations on the fine structure of blood capillaries. *The peripheral blood vessels*, 17-44.

Feng, Y., Varikooty, J., & Simpson, T. L. (2001). Diurnal variation of corneal and corneal epithelial thickness measured using optical coherence tomography. *Cornea, 20*(5), 480-483.

Fercher, A. F., Drexler, W., Hitzenberger, C. K., & Lasser, T. (2003). Optical coherence tomography - principles and applications. *Reports on Progress in Physics, 66*(2), 239-303.

Fercher, A. F., Hitzenberger, C. K., Kamp, G., & El-Zaiat, S. Y. (1995). Measurement of intraocular distances by backscattering spectral interferometry. *Optics Communications, 117*(1), 43-48.

Fercher, A. F., Mengedoht, K., & Werner, W. (1988). Eye-length measurement by interferometry with partially coherent light. *Optics Letters, 13*(3), 186-188.

Fercher, A. F., & Roth, E. (1986, September). Ophthalmic laser interferometry. In *1986 International Symposium/Innsbruck* (pp. 48-51). International Society for Optics and Photonics.

Fitzgerald, J. P., & Efron, N. (1986). Oxygen uptake profile of the human cornea. *Clinical and Experimental Optometry, 69*(4), 149-152.

Foster, F. S., Pavlin, C. J., Harasiewicz, K. A., Christopher, D. A., & Turnbull, D. H. (2000). Advances in ultrasound biomicroscopy. *Ultrasound in Medicine & Biology, 26*(1), 1-27.

Fujimoto, J. (2006, May). Optical coherence tomography. In *Conference on Lasers and Electro-Optics*. Optical Society of America.

Furness, J. B. (1973). Arrangement of blood vessels and their relation with adrenergic nerves in the rat mesentery. *Journal of Anatomy, 115*(Pt 3), 347-364.

Furness, J. B., & Marshall, J. M. (1974). Correlation of the directly observed responses of mesenteric vessles of the rat to nerve stimulation and noradrenaline with the distribution of adrenergic nerves. *The Journal of Physiology*, *239*(1), 75-88.

Gipson, I. K. (1989). The epithelial basement membrane zone of the limbus. *Eye*, *3*(2), 132-140.

Gong, H., Tripathi, R. C., & Tripathi, B. J. (1996). Morphology of the aqueous outflow pathway. *Microscopy research and technique*, *33*(4), 336-367.

Gould, D. B., Smith, R. S., & John, S. (2004). Anterior segment development relevant to glaucoma. *Int J DevBiol*, *48*(8-9), 1015-1029.

Granger, H. J., Borders, J. L., Meininger, G. A., Goodman, A. H., & Barnes, G. E. (1983). Microcirculatory control systems. *The Physiology and Pharmacology of the Microcirculation*, *1*, 209-236.

Granger, H. J., Schelling, M. E., Lewis, R. E., Zawieja, D. C., &Meininger, C. J. (1988). Physiology and pathobiology of the microcirculation. *American Journal of Otolaryngology*, *9*(6), 264-277.

Grulkowski, I., Gora, M., Szkulmowski, M., Gorczynska, I., Szlag, D., Marcos, S., Kowalczyk, A., & Wojtkowski, M. (2009). Anterior segment imaging with Spectral OCT system using a high-speed CMOS camera. *Optics express*, *17*(6), 4842-4858.

Grulkowski, I., Liu, J. J., Baumann, B., Potsaid, B., Lu, C., & Fujimoto, J. G. (2011). Imaging limbal and scleral vasculature using swept source optical coherence tomography. *Photonics Letters of Poland, 3*(4), 132-134.

Grulkowski, I., Liu, J. J., Potsaid, B., Jayaraman, V., Lu, C. D., Jiang, J., Cable, A. E., & Fujimoto, J. G. (2012). Retinal, anterior segment and full eye imaging using ultrahigh speed swept source OCT with vertical-cavity surface emitting lasers. *Biomedical optics express*, *3*(11), 2733.

Hamanaka, T., Bill, A., Ichinohasama, R., & Ishida, T. (1992). Aspects of the development of Schlemm's canal. *Experimental Eye Research, 55*(3), 479-488.

Han, M., Giese, G., &Bille, J. (2005). Second harmonic generation imaging of collagen fibrils in cornea and sclera. *Optics Express, 13*(15), 5791-5797.

Hanna, C., Bicknell, D. S., & O'Brien, J. E. (1961). Cell turnover in the adult human eye.*Archives of Ophthalmology, 65*(5), 695.

Hogan, M. J., Alvarado, J. A., & Weddell, J. E. (1971). In Alvarado J. A., Weddell J. E. (Eds.), *Histology of the human eye: An atlas and textbook, (pp.112 -182)*. Philadelphia ; Saunders, 1971.

Hong, C., Arosemena, A., Zurakowski, D., & Ayyala, R. S. (2005). Glaucoma drainage devices: A systematic literature review and current controversies. *Survey of Ophthalmology, 50*(1), 48-60.

Huang, D., Swanson, E. A., Lin, C. P., Schuman, J. S., Stinson, W. G., Chang, W., & Puliafito, C. A. (1991). Optical coherence tomography. *Science, 254*(5035), 1178-1181.

Hulst, H. C. (1957). *Light scattering: by small particles*. Courier Dover Publications, pp. 3 - 15.

Hutchings, N., Hyun, C., Bizheva, K., & Simpson, T. L. (2010). Accuracy and repeatability of ultra-high resolution optical coherence tomography [Abstract]. *5685*(D838)

Hutchings, N., Simpson, T. L., Hyun, C., Moayed, A. A., Hariri, S., Sorbara, L., & Bizheva, K. (2010). Swelling of the human cornea revealed by high-speed, ultrahigh-resolution optical coherence tomography. *Investigative ophthalmology & visual science*, *51*(9), 4579-4584.

Ishikawa, H., Inazumi, K., Liebmann, J. M., & Ritch, R. (2000). Inadvertent corneal indentation can cause artifactitious widening of the iridocorneal angle on ultrasound biomicroscopy. *Ophthalmic Surgery and Lasers, 31*(4), 342-345.

Ishikawa, H., & Schuman, J. S. (2004). Anterior segment imaging: ultrasound biomicroscopy. *Ophthalmology Clinics of North America*, *17*(1), 7.

Iwamoto, T., & Smelser, G. K. (1965). Electron microscope studies on the mast cells and blood and lymphatic capillaries of the human corneal limbus. *Investigative Ophthalmology & Visual Science*, *4*(5), 815-834.

Jahrling, R. C. (1999). Role of the ocularist. *Enucleation, Evisceration and Exenteration of the Eye.Boston, MA: Butterworth Heinemann, p18-21.*

Johnson, M., & Kamm, R. (1983). The role of Schlemm's canal in aqueous outflow from the human eye. *Investigative Ophthalmology & Visual Science*, *24*(3), 320-325.

Karnowski, K., Kaluzny, B. J., Szkulmowski, M., Gora, M., &Wojtkowski, M. (2011). Corneal topography with high-speed swept source OCT in clinical examination. *Biomedical Optics Express*, *2*(9), 2709-2720.

Kaufman, P. L., Levin, L. A., Alm, A., Nilsson, S. F., & Ver Hoeve, J. (Eds.). (2011). *Adler's Physiology of the Eye*. Elsevier Health Sciences, pp. 243-270.

Kehlet Barton, J., Izatt, J. A., Kulkarni, M. D., Yazdanfar, S., & Welch, A. J. (1999). Three-dimensional reconstruction of blood vessels from in vivo color doppler optical coherence tomography images. *Dermatology, 198*(4), 355-361.

Khan, F. A., Niazi, S. P. K., & Awan, S. (2012). The clinical significance of perilimbal conjunctival pigmentation in vernal conjunctivitis. *Journal of the College of Physicians and Surgeons--Pakistan: JCPSP*, *22*(1), 19.

Konstantopoulos, A., Hossain, P., & Anderson, D. F. (2007). Recent advances in ophthalmic anterior segment imaging: a new era for ophthalmic diagnosis?. *British Journal of Ophthalmology*, *91*(4), 551-557.

Krohn, J., & Bertelsen, T. (1998). Light microscopy of uveoscleral drainage routes after gelatine injections into the suprachoroidal space. *Acta Ophthalmologica Scandinavica*, *76*(5), 521-527.

Kronfeld, P. C. (1948). Gonioscopic studies of the canal of Schlemm. *American Journal of Ophthalmology, 31*(11), 1507.

Kronfeld, P. C. (1949). Further gonioscopic studies on the canal of Schlemm. *Archives of Ophthalmology, 41*(4), 393-405.

Leitgeb, R., Hitzenberger, C., & Fercher, A. (2003). Performance of fourier domain vs. time domain optical coherence tomography. *Optics Express, 11*(8), 889-894.

Lepple-Wienhues, A., Stahl, F., & Wiederholt, M. (1991). Differential smooth muscle-like contractile properties of trabecular meshwork and ciliary muscle. *Experimental Eye Research, 53*(1), 33-38.

Li, P., An, L., Reif, R., Shen, T. T., Johnstone, M., & Wang, R. K. (2011). In vivo microstructural and microvascular imaging of the human corneo-scleral limbus using optical coherence tomography. *Biomedical Optics Express, 2*(11), 3109.

Liu, Z., Huang, A. J., & Pflugfelder, S. C. (1999). Evaluation of corneal thickness and topography in normal eyes using the orbscan corneal topography system. *The British Journal of Ophthalmology, 83*(7), 774-778.

Liu, Z., Xie, Y., & Zhang, M. (2001). Corneal topography and pachymetry in normal eyes. *[Zhonghua Yan KeZaZhi] Chinese Journal of Ophthalmology, 37*(2), 125-128.

Marfurt, C. F., Cox, J., Deek, S., & Dvorscak, L. (2010). Anatomy of the human corneal innervation. *Experimental Eye Research, 90*(4), 478-492.

Meyer, P. A. (1989). The circulation of the human limbus. *Eye, 3*(2), 121-127.

Molteno, A. (1969). New implant for drainage in glaucoma.clinical trial. *The British Journal of Ophthalmology, 53*(9), 606.

Morrison, J. C., & Van Buskirk, E. M. (1983). Anterior collateral circulation in the primate eye. *Ophthalmology, 90*(6), 707-715.

Moses, R. A., Hoover, G. S., & Oostwouder, P. H. (1979). Blood reflux in Schlemm's canal: I. normal findings. *Archives of Ophthalmology, 97*(7), 1307.

Müller, L. J., Marfurt, C. F., Kruse, F., & Tervo, T. M. (2003). Corneal nerves: Structure, contents and function. *Experimental Eye Research, 76*(5), 521-542.

Neri, A., Malori, M., Scaroni, P., Leaci, R., Delfini, E., & Macaluso, C. (2012). Corneal thickness mapping by 3D swept-source anterior segment optical coherence tomography. *Acta Ophthalmologica, 90*(6), e452-7.

Niederer, R. L., & McGhee, C. N. (2010). Clinical in vivo confocal microscopy of the human cornea in health and disease. *Progress in Retinal and Eye Research, 29*(1), 30-58.

Ockert, C. E. (1968). Speed of light. *American Journal of Physics, 36*, 158-159.

Owen, C. G., Fitzke, F. W., & Woodward, E. G. (1996). A new computer assisted objective method for quantifying vascular changes of the bulbar conjunctivae. *Ophthalmic and Physiological Optics, 16*(5), 430-437.

Oyster, C. W. (1999).*The human eye: Structure and function*. Sunderland, Mass.,Sinauer Associates, pp. 260-271, 390-409.

Papas, E. B. (2003). The limbal vasculature. *Contact Lens and Anterior Eye, 26*(2), 71-76.

Papas, E. (1998). On the relationship between soft contact lens oxygen transmissibility and induced limbal hyperaemia. *Experimental Eye Research, 67*(2), 125-131.

Papas, E. B., Vajdic, C. M., Austen, R., & Holden, B. A. (1997). High-oxygen-transmissibility soft contact lenses do not induce limbal hyperaemia. *Current Eye Research, 16*(9), 942-948.

Patel, D. V., & McGhee, C. N. (2007). Contemporary in vivo confocal microscopy of the living human cornea using white light and laser scanning techniques: A major review. *Clinical & Experimental Ophthalmology, 35*(1), 71-88.

Pavlin, C. J., & Foster, F. S. (1995). *Ultrasound biomicroscopy of the eye* (pp. 140-154). New York: Springer-Verlag.

Pavlin, C., Harasiewicz, K., Sherar, M., & Foster, F. (1991).Clinical use of ultrasound biomicroscopy. *Ophthalmology, 98*(3), 287-295.

Pavlin, C. J., & Foster, F. S. (1998). Ultrasound biomicroscopy.high-frequency ultrasound imaging of the eye at microscopic resolution. *Radiologic Clinics of North America, 36*(6), 1047-1058.

Pavlin, C. J., Sherar, M. D., & Foster, F. S. (1990). Subsurface ultrasound microscopic imaging of the intact eye. *Ophthalmology, 97*(2), 244-250.

Pawley, J. B. (Ed.). (1995). *Handbook of biological confocal microscopy* (pp. 3-15). Springer.

Pawley, J. B. (2006). Fundamental limits in confocal microscopy. *Handbook of biological confocal microscopy* (pp. 20-42). Springer.

Perona, P., & Malik, J. (1990). Scale-space and edge detection using anisotropic diffusion. *Pattern Analysis and Machine Intelligence, IEEE Transactions On, 12*(7), 629-639.

Petroll, W. M., Jester, J. V., & Cavanagh, H. D. (1994). In vivo confocal imaging: General principles and applications. *Scanning, 16*(3), 131-149.

Ragan, D. M., Schmidt, E. E., MacDonald, I. C., & Groom, A. C. (1988). Spontaneous cyclic contractions of the capillary wall in vivo, impeding red cell flow: A quantitative analysis. evidence for endothelial contractility. *Microvascular Research, 36*(1), 13-30.

Ramos, J. L. B., Li, Y., & Huang, D. (2009). Clinical and research applications of anterior segment optical coherence tomography - a review. *Clinical & Experimental Ophthalmology, 37*(1), 81.

Reinstein, D. Z., Silverman, R. H., Rondeau, M. J., & Coleman, D. J. (1994). Epithelial and corneal thickness measurements by high-frequency ultrasound digital signal processing. *Ophthalmology, 101*(1), 140-146.

Reinstein, D. Z., Silverman, R. H., Trokel, S. L., & Coleman, D. J. (1994). Corneal pachymetric topography. *Ophthalmology, 101*(3), 432-438.

Remon, L., Cristobal, J. A., Castillo, J., Palomar, T., Palomar, A., & Perez, J. (1992). Central and peripheral corneal thickness in full-term newborns by ultrasonic pachymetry. *Investigative Ophthalmology & Visual Science, 33*(11), 3080-3083.

Ritch, R., & Klein, E. E. (1990).Transscleral drainage implant device for the treatment of glaucoma. *U.S. Patent 4,968,296.*

Rohlf, F. J., &Bookstein, F. L. (1990). *Proceedings of the Michigan morphometrics workshop* (pp. 77–122). University of Michigan, Museum of Zoology.

Romano, A. C., Espana, E. M., Yoo, S. H., Budak, M. T., Wolosin, J. M., & Tseng, S. C. (2003). Different cell sizes in human limbal and central corneal basal epithelia measured by confocal microscopy and flow cytometry. *Investigative Ophthalmology & Visual Science, 44*(12), 5125-5129.

Sakata, L. M., DeLeon-Ortega, J., Sakata, V., & Girkin, C. A. (2009). Optical coherence tomography of the retina and optic nerve–a review. *Clinical & experimental ophthalmology*, *37*(1), 90-99

Schmetterer, L., & Kiel, J. W. (Eds.). (2009). *Ocular blood flow (pp. 4-6).* Springer.

Schmitt, J. M. (1999). Optical coherence tomography (OCT): A review. *Selected Topics in Quantum Electronics, IEEE Journal Of, 5*(4), 1205-1215.

Schneider, C. A., Rasband, W. S., & Eliceiri, K. W. (2012). NIH image to ImageJ: 25 years of image analysis. *Nature Methods, 9*(7), 671-675.

Shi, G., Wang, F., Li, X., Lu, J., Ding, Z., Sun, X., & Zhang, Y. (2012). Morphometric measurement of schlemm's canal in normal human eye using anterior segment swept source optical coherence tomography. *Journal of Biomedical Optics*, *17*(1), 0160161-0160164.

Simpson, T., & Fonn, D. (2008). Optical coherence tomography of the anterior segment. *The Ocular Surface*, *6*(3), 117-127.

Simpson, T., Bizheva, K., Feng, Y., Alabi, E., & Hutchings, N. (2012). The limbal epithelial and vascular structure under the upper eye lid, characterized using UHR-OCT. [Abstract]. *ARVO Poster*, *105*(A248)

Smith, R. S., Zabaleta, A., Kume, T., Savinova, O. V., Kidson, S. H., Martin, J. E., & John, S. W. (2000). Haploinsufficiency of the transcription factors FOXC1 and FOXC2 results in aberrant ocular development. *Human Molecular Genetics, 9*(7), 1021-1032.

Steinert, R. F., & Huang, D. (2008). In Steinert R. F., Huang D. (Eds.), *Anterior segment optical coherence tomography, pp. 21 -50*. Thorofare, NJ, Slack.

Stemler, S. E. (2004). A comparison of consensus, consistency, and measurement approaches to estimating interrater reliability. *Practical Assessment, Research & Evaluation, 9*(4), 66-78.

Stern, M. E., Beuerman, R. W., Fox, R. I., Gao, J., Mircheff, A. K., & Pflugfelder, S. C. (1998). The pathology of dry eye: The interaction between the ocular surface and lacrimal glands. *Cornea, 17*(6), 584-589.

Swanson, E. A., Izatt, J. A., Hee, M. R., Huang, D., Lin, C. P., Schuman, J. S., Puliafito, C. A., & Fujimoto, J. G. (1993a). In vivo retinal imaging by optical coherence tomography. *Optics Letters, 18*(21), 1864-1866.

Swanson, E. A., Izatt, J. A., Hee, M. R., Huang, D., Lin, C. P., Schuman, J. S., Puliafito, C. A., & Fujimoto, J. G. (1993b). In vivo retinal imaging by optical coherence tomography. *Optics Letters, 18*(21), 1864-1869.

Thevenaz, P., Ruttimann, U. E., & Unser, M. (1998). A pyramid approach to subpixel registration based on intensity. *IEEE Transactions on Image Processing : A Publication of the IEEE Signal Processing Society, 7*(1), 27-41.

Townsend, W. M. (1991). The limbal palisades of Vogt. *Transactions of the American Ophthalmological Society, 89,* 721.

Turtz, A. I., & Fisher, Y. L. (1979). Slit-lamp biomicroscopy. *Annals of Plastic Surgery, 2*(2), 177-179.

Van Buskirk, E. M. (1989). The anatomy of the limbus. *Eye, 3*(2), 101-108.

van der Merwe, E. L., & Kidson, S. H. (2010). Advances in imaging the blood and aqueous vessels of the ocular limbus. *Experimental Eye Research, 91*(2), 118-126.

vanVelthoven, M. E. J., Faber, D. J., Verbraak, F. D., van Leeuwen, T. G., & de Smet, M. D. (2007). Recent developments in optical coherence tomography for imaging the retina. *Progress in Retinal and Eye Research, 26*(1), 57-77.

Vasudevan, B., Simpson, T. L., & Sivak, J. G. (2008). Regional variation in the refractive-index of the bovine and human cornea. *Optometry & Vision Science, 85*(10), 977-981.

Wang, N., Chintala, S. K., Fini, M. E., & Schuman, J. S. (2001). Activation of a tissue-specific stress response in the aqueous outflow pathway of the eye defines the glaucoma disease phenotype. *Nature Medicine, 7*(3), 304-309.

Wiedeman, M. P. (1968). Blood flow through terminal arterial vessels after denervation of the bat wing. *Circulation Research, 22*(1), 83-89.

Zhang, X., Li, Q., Liu, B., Zhou, H., Wang, H., Zhang, Z., & Zou, H. (2011). In vivo cross-sectional observation and thickness measurement of bulbar conjunctiva using optical coherence tomography. *Investigative Ophthalmology & Visual Science, 52*(10), 7787-7791.